Resource Allocation and Beamforming Design for Active STAR-RIS-Assisted Wireless-Powered MEC

Xintong Qin, Wenjuan Yu, *Member, IEEE*, Qiang Ni, *Senior Member, IEEE*, Zhengyu Song, *Member, IEEE*, Tianwei Hou, *Member, IEEE*, Jun Wang, and Xin Sun

***Abstract*—To address the issues of limited computational capability and constrained battery life faced by users in the Internet of Things, wireless-powered mobile edge computing (MEC) has been proposed as a promising solution. However, the efficiency of its key functions, namely task offloading and energy transfer, can be significantly impaired if the direct links between the access point (AP) and users are obstructed. Inspired by the potentials of active simultaneous transmission and reflection reconfigurable intelligent surface (STAR-RIS) for achieving full-space coverage and mitigating multiplicative fading effects, this paper investigates the incorporation of active STAR-RIS in wireless-powered MEC. To meet the high data rate requirements in future smart environments, we aim to maximize the total number of completed task bits. To address the formulated challenging non-convex problem, a resource allocation and active beamforming algorithm (RAABA) is first proposed for a basic two-user non-orthogonal multiple access (NOMA) scenario, jointly optimizing the energy transfer time, decoding order, transmit power, CPU frequency of users, and beamforming of STAR-RIS. We then extend the RAABA to general multi-user scenarios (RAABAM) by leveraging a matching-theory-based user pairing algorithm. Furthermore, a low-complexity RAABAM (L-RAABAM) is proposed by simplifying the matching process and deriving a closed-form expression for the optimal transmit power of users. Simulation results show that: i) by jointly optimizing multiple highly-coupled variables, our proposed RAABAM and L-RAABAM schemes achieve a higher total number of completed task bits; ii) the active STAR-RIS significantly outperforms passive/active traditional RIS and passive STAR-RIS; iii) the deployment rules for active STAR-RIS differ from those for passive STAR-RIS in wireless-powered MEC, where the optimal deployment location of active STAR-RIS depends on the number of its elements.**

***Index Terms*—Resource allocation, beamforming design, wireless-powered MEC, non-orthogonal multiple access (NOMA), active simultaneous transmission and reflection reconfigurable intelligent surface (STAR-RIS).**

Manuscript received December 5, 2024; revised July 30, 2025; accepted September 17, 2025. Date of publication September 17, 2025; date of current version September 17, 2025. This work was supported in part by the National Natural Science Foundation of China under Grant 61901027, and in part by the UK EPSRC CHEDDAR Communications Hub under Grant EP/X040518/1 and EP/Y037421/1. The associate editor coordinating the review of this article and approving it for publication was Chih-Yu Wang. *(Corresponding author: Zhengyu Song.)*

X. Qin, Z. Song, T. Hou, J. Wang, and X. Sun are with the School of Electronic and Information Engineering, Beijing Jiaotong University, Beijing 100044, China (e-mails: 20111046@bjtu.edu.cn, songzy@bjtu.edu.cn, twhou@bjtu.edu.cn, wangjun1@bjtu.edu.cn, xsun@bjtu.edu.cn).

W. Yu and Q. Ni are with the School of Computing and Communications, InfoLab21, Lancaster University, Lancaster LA1 4WA, U.K. (e-mails: w.yu8@lancaster.ac.uk, q.ni@lancaster.ac.uk).

I. Introduction

The swift advancement of the Internet of Things (IoT) has precipitated a significant rise in the proliferation of smart devices, like smart home systems, wearable health monitors, etc. [1]. To support the sophisticated operation and achieve advanced functionalities, smart IoT devices are often engaged in computation-intensive and latency-sensitive tasks such as real-time data processing and immediate decision-making. Nevertheless, due to the inherent limitations in power storage and computational capacity, IoT devices are unable to effectively meet the communication and computation demands of complex tasks. To overcome these challenges, mobile edge computing (MEC) and wireless power transfer (WPT) are considered pivotal technologies for next-generation communication systems [2] [3]. MEC provides powerful computing capabilities by bringing MEC servers in close proximity to users, while WPT enables users to harvest energy from radio frequency (RF) signals for information processing and transmission. Recognizing the dual demands for energy and computational capacity in emerging applications such as smart transportation [4], smart cities [5], wearable devices and smart home [6], [7], the integration of MEC and WPT, known as the wireless-powered MEC, has garnered significant interests. Such integration promises to enhance computational performance and extend the operational lifetime of IoT devices, thereby effectively addressing their resource constraints [8].

As a crucial innovation for future smart environments, wireless-powered MEC has been extensively studied in recent literature. For example, in [9], the computation rate maximization for wireless-powered MEC is investigated by using the alternating direction method of multipliers (ADMM) technique, where the time allocation, computing mode selection, and CPU frequency are jointly optimized. In [10], a Dinkelbach-based algorithm is proposed to jointly optimize communication and computation resources to maximize the computation energy efficiency for wireless-powered MEC under the non-orthogonal multiple access (NOMA) protocol. Simulation results demonstrate that the proposed NOMA scheme outperforms orthogonal multiple access (OMA). Furthermore, in order to solve the non-convex resource allocation problems with lower complexity, deep reinforcement learning methods have been proposed for wireless-powered MEC, such as the deep neural network (DNN)-based method [11], deep Q-network (DQN)-based method [12], and the deep deterministic policy gradient (DDPG)-based method [13].

Despite the advantages of wireless-powered MEC in en-

hancing users' computing capabilities and operational lifetimes, its full potentials have not been fully exploited, primarily because the communication links between the access point (AP) and users are often imperfect. For example, in a smart city, the direct links between wireless sensors and AP may be blocked by high-rise buildings, urban infrastructures, or dynamically changing environments, posing significant challenges for downlink energy transfer and uplink task offloading. To enhance both uplink and downlink channel conditions, the reconfigurable intelligent surface (RIS), characterized by its capability to smartly reconfigure the wireless propagation environment [14], [15], has recently been introduced to assist both energy transfer and task offloading in wireless-powered MEC systems.

To fully exploit the benefits of RIS, the beamforming of RIS should be jointly designed with the resource allocation in wireless-powered MEC, making the formulated optimization problems more challenging. Therefore, in [16] and [17], the joint resource allocation and beamforming design for RIS-assisted wireless-powered MEC is solved using the block coordinate descent (BCD) technique. It is found that RIS can achieve significant performance gains by adjusting the phase shift to improve the channel conditions. When employing the NOMA protocol for RIS-assisted wireless-powered MEC, the uplink beamforming design of RIS would be more difficult since the phase shift adjustment must simultaneously accommodate multiple signals with varying angles of incidence. To tackle this challenge, in [18], the successive convex approximation (SCA) and penalty methods are utilized to solve the non-convex optimization problem related to RIS's beamforming design with NOMA protocol. Although NOMA outperforms OMA in RIS-assisted wireless-powered MEC, the performance gain can be further improved by optimizing the user pairing strategy. Nevertheless, the user pairing problem under the NOMA protocol is a NP-hard problem, which is intractable to obtain the optimal user pairing scheme in polynomial complexity. Although several feasible approaches have been proposed by existing studies, such as the relaxation-based method [19], deep learning algorithms [20], and channel-gain-based algorithm [21], the user pairing problem in RIS-assisted wireless powered MEC systems is still an open problem.

It is worth noting that since RIS can only reflect the incident signals, the users and AP have to be located at the same side of RIS, which means RIS can only achieve half-space coverage. To address the geographical limitation of RIS, the simultaneously transmitting and reflecting RIS (STAR-RIS) has been proposed recently [22]–[26]. By manipulating both electric and magnetic currents, the STAR-RIS can simultaneously reflect and transmit signals, achieving full-space coverage and providing extra degrees of freedoms (DoFs) to further improve channel conditions. By leveraging the advantages of STAR-RIS, a STAR-RIS-assisted wireless-powered MEC model is proposed in [27], where the STAR-RIS is deployed to assist task offloading and energy harvesting for all users in full-space. Similarly, in [28], the computation rate maximization problems are investigated for STAR-RIS-assisted wireless-powered MEC. Simulation results illustrate that STAR-RIS can significantly increase the computation rate for wireless-powered MEC compared to traditional reflecting-only RIS.

Although STAR-RIS can provide additional reflected or transmitted links for all users in wireless-power MEC systems, the received signals of both the users and AP still suffer from product path loss attenuation, i.e., multiplicative fading effects, which heavily restrict the potentials of STAR-RIS [29]. Fortunately, active STAR-RIS is a promising approach to overcome the multiplicative fading effects. Compared to passive STAR-RIS, active STAR-RIS goes beyond phase shift configuration, and can amplify the incident signals to further improve the strength of received signals [30]. With the assistance of active STAR-RIS, the energy and computation requirements in wireless-powered MEC can be better satisfied, especially in the scenarios where the direct links between users and AP are blocked. Hence, given the potential gains of active STAR-RIS, it is imperative to integrate active STAR-RIS into the wireless-powered MEC.

However, to the best of our knowledge, several key problems remain unsolved in this field. Firstly, unlike passive STAR-RIS, active STAR-RIS amplifies not only the incident signals but also the noise. Thus, the beamforming design of active STAR-RIS must carefully manage the trade-off between amplified noise power and received signal power. Additionally, although the resource allocation problems have been well investigated in wireless-powered MEC, such as in [9]–[13], the proposed algorithms in related works cannot be directly applied to active STAR-RIS-assisted wireless-powered MEC, since the beamforming of active STAR-RIS is highly coupled with AP's energy transfer time and users' transmit power. How to achieve joint resource allocation and beamforming design to fully exploit the advantages of active STAR-RIS in wireless-powered MEC requires further investigation. Secondly, since the noise power amplified by active STAR-RIS also attenuates with distance, the deployment rules for passive STAR-RIS may not hold for active STAR-RIS. Thus, in order to alleviate the impact of amplified noise on users' task offloading, the deployment location of the active STAR-RIS in wireless-powered MEC should be carefully designed. Thirdly, when applying NOMA in wireless-powered MEC with passive STAR-RIS, user pairing algorithm can be designed solely based on users' channel gains since the noise of passive STAR-RIS can be ignored [27], [31]. However, the noise amplified by active STAR-RIS cannot be overlooked, and the amplified noise power varies on each side of active STAR-RIS, which poses additional challenges for user pairing of NOMA.

Motivated by the above observations and different from related works, in this paper, we investigate the joint resource allocation and beamforming design for active STAR-RIS-assisted wireless-powered MEC systems under NOMA protocol, aiming to maximize the total number of completed task bits. The main contributions of this paper are summarized as follows.

1) A novel active STAR-RIS-assisted wireless-powered MEC model is proposed, where the AP first transfers energy to users, and then users can offload task bits to the AP for computing by utilizing the harvested energy. The active STAR-RIS which can reflect/transmit and amplify signals, is deployed to mitigate the multiplicative fading effect and enhance the

channel gains between AP and users. Under the NOMA protocol, optimization problems are formulated to maximize the total number of completed task bits for both two-user and multi-user scenarios.

2) For the two-user scenario, to solve the formulated challenging non-convex problem, we propose a resource allocation and active beamforming algorithm (RAABA) to jointly optimize the energy transfer time, decoding order, transmit power, CPU frequency of users, and the beamforming of active STAR-RIS. The energy transfer time and CPU frequency are updated using closed-form expressions, while the users' transmit power optimization and active STAR-RIS's beamforming design are based on the Lagrangian dual method and quadratic transform, respectively. The proposed RAABA is then extended to general multi-user scenarios (RAABAM) by leveraging a matching-theory-based user pairing algorithm. Finally, by further modifying the matching process and deriving the closed-form expression for users' transmit power, a low-complexity RAABAM (L-RAABAM) is proposed for multi-user scenarios.

3) Simulation results show that: i) our proposed RAABAM and L-RAABAM perform close to the exhaustive search method and much better than the random pairing and channel-gain-based algorithms; ii) the active STAR-RIS achieves a higher total number of completed task bits than the passive/active traditional RIS and passive STAR-RIS; iii) interestingly, the best location to deploy active STAR-RIS depends on the number of elements. When the active STAR-RIS has a larger number of elements, the total number of completed task bits increases as the STAR-RIS is deployed closer to users.

The structure of the paper is as follows. Section II presents the system model for active STAR-RIS-assisted wireless-powered MEC. In Section III, we detail the proposed algorithms designed for both two-user and multi-user scenarios. Section IV provides numerical results to validate our proposed algorithms, and Section V concludes the paper.

II. System Model

As shown in Fig. 1, we consider a wireless-powered MEC system assisted by an active STAR-RIS with M elements. The AP is equipped with an MEC server and an RF energy transmitter to provide computing services and energy supplies for users. The users are indexed by $i \in \mathcal{I} = \{1, 2, ..., I\}$. During the given mission period T, with the help of active STAR-RIS, the AP first transmits power to all users, and then the users utilize the harvested energy to offload task bits to the AP. The energy transfer time is given by τ. During the period of energy transfer, the beamforming matrix of STAR-RIS is denoted as $\mathbf{u}_{\mathrm{RIS}}^{D,e} = \mathrm{diag}\left(\boldsymbol{\varphi}_{\mathrm{RIS}}^{\mathrm{D},e}\right) \in \mathbb{C}^{M\times M}$, where $e = \{r, t\}$, and $\boldsymbol{\varphi}_{\mathrm{RIS}}^{D,e} = \left[\sqrt{\beta_1^{D,e}} e^{j\theta_1^{D,e}}, \sqrt{\beta_2^{D,e}} e^{j\theta_2^{D,e}}, ..., \sqrt{\beta_M^{D,e}} e^{j\theta_M^{D,e}}\right]$ [22], [32]. Based on the location of STAR-RIS, if the user is located at the reflection space, we have $e = r$. Otherwise, $e = t$. $\theta_m^{D,e}$ and $\beta_m^{D,e}$ are the phase shift and amplitude for the m-th element of STAR-RIS, with $\theta_m^{D,e} \in [0, 2\pi)$ and $\beta_m^{D,e} \in [0, \beta_{\max}]$, $\forall m \in \mathcal{M} = \{1, 2, ..., M\}$. Since the active STAR-RIS can achieve the signal amplification, we have $\beta_{\max} > 1$.

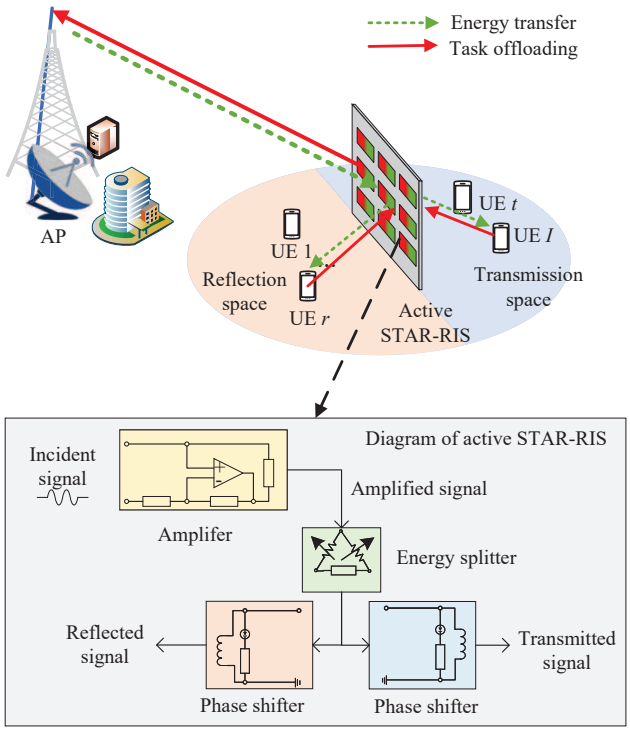

Fig. 1. The active STAR-RIS-assisted wireless-powered MEC system.

When the AP transmits the energy-carrying signal z_{AP} to users, the direct links among the AP and users are assumed to be blocked by obstacles, which is a typical scenario where the deployment of STAR-RIS is essential [33]. In this scenario, the full-space coverage provided by STAR-RIS can also be fully exploited. The Rician fading channel model are adopted for all channels involved in this paper, and it is assumed that the AP can obtain the perfect channel state information through advanced channel estimation technologies. The downlink channels from AP to the STAR-RIS and that from STAR-RIS to user i are given by [34]

$$\begin{aligned} \mathbf{h}_{\mathrm{AP,RIS}}^{D} &= \sqrt{\frac{\varpi_{\mathrm{AP}}^{D}}{1+\varpi_{\mathrm{AP}}^{D}}}\mathbf{h}_{\mathrm{AP,RIS}}^{D,\mathrm{LoS}} + \sqrt{\frac{1}{1+\varpi_{\mathrm{AP}}^{D}}}\mathbf{h}_{\mathrm{AP,RIS}}^{D,\mathrm{NLoS}}, \\ \mathbf{h}_{\mathrm{RIS},i}^{D} &= \sqrt{\frac{\varpi_{\mathrm{RIS}}^{D}}{1+\varpi_{\mathrm{RIS}}^{D}}}\mathbf{h}_{\mathrm{RIS},i}^{D,\mathrm{LoS}} + \sqrt{\frac{1}{1+\varpi_{\mathrm{RIS}}^{D}}}\mathbf{h}_{\mathrm{RIS},i}^{D,\mathrm{NLoS}}, \end{aligned} \tag{1}$$

where ϖ_{AP}^{D} and $\varpi_{\mathrm{RIS}}^{D}$ represent the corresponding Rician factors. $\mathbf{h}_{\mathrm{AP,RIS}}^{D,\mathrm{LoS}}$ and $\mathbf{h}_{\mathrm{RIS},i}^{D,\mathrm{LoS}}$ are line-of-sight (LoS) components. $\mathbf{h}_{\mathrm{AP,RIS}}^{D,\mathrm{NLoS}}$ and $\mathbf{h}_{\mathrm{RIS},i}^{D,\mathrm{NLoS}}$ indicate the non-LoS (NLoS) components. Thus, the energy-carrying signal reflected/transmitted and amplified by the STAR-RIS can be expressed as $z_{\mathrm{RIS}}^{D} = \mathbf{u}_{\mathrm{RIS}}^{D,e}\mathbf{h}_{\mathrm{AP,RIS}}^{D} z_{\mathrm{AP}} + n_{\mathrm{RIS}}$, where n_{RIS} is the thermal noise at the STAR-RIS. Then, the signal received by user i can be expressed as $y_i^{D} = \mathbf{h}_{\mathrm{RIS},i}^{D} z_{\mathrm{RIS}} + n_i$, where n_i is the additive white Gaussian noise (AWGN) at user i.

Hence, the received RF power at user i can be expressed as

$$P_{\mathrm{input},i} = P_{\mathrm{AP}} \left| \mathbf{h}_{\mathrm{RIS},i}^{D}\mathbf{u}_{\mathrm{RIS}}^{D,e}\mathbf{h}_{\mathrm{AP,RIS}}^{D} \right|^2 + n_{\mathrm{RIS}}^2 \left\| \mathbf{u}_{\mathrm{RIS}}^{D,e} \right\|^2, \tag{2}$$

where P_{AP} is the transmit power of AP.

In this paper, we adopt a non-linear energy harvesting model to characterize the energy conversion behavior at users. Compared to traditional linear energy harvesting model where the harvested power is assumed to be proportional to the received RF power, the non-linear energy harvesting model takes the circuit saturation effects into consideration, which can prevent the overestimation of the harvested energy [35]. Based on the non-linear energy harvesting model, the harvested power of user i can be given by

$$P_{\mathrm{out},i}=\frac{\upsilon}{(1-\chi)\left(1+\exp\left(-\psi\left(P_{\mathrm{input},i}-\phi\right)\right)\right)}-\frac{\upsilon\chi}{(1-\chi)}, \quad (3)$$

where $\chi = 1/(1+\exp(\psi\phi))$. υ indicates the maximum harvested power at users when the circuit is saturated. ψ and ϕ are constants related to the detailed circuit specifications. The total energy harvested by users i in the mission period can be given by $\tau P_{\mathrm{out},i}$.

In the rest of mission period, the users will simultaneously perform task offloading and local computing by utilizing the harvested energy. Specifically, denote the CPU frequency of user i for local computing as f_i. Then, the amount of task bits that user i can complete during the mission period can be given by

$$L_i^{\mathrm{local}} = \frac{f_i\left(T-\tau\right)}{C_i}, \quad (4)$$

where C_i is the CPU cycles required for computing 1-bit of task-input data. The energy consumption of user i for local computing can be expressed as

$$E_i^{\mathrm{local}} = \kappa\left(T-\tau\right)f_i^3, \quad (5)$$

where κ is the effective capacitance coefficient.

During the period of uplink task offloading, the beamforming matrix of STAR-RIS is given by $\mathbf{u}_{\mathrm{RIS}}^{U,e} = \mathrm{diag}\left(\boldsymbol{\varphi}_{\mathrm{RIS}}^{U,e}\right) \in \mathbb{C}^{M\times M}$, where $e=\{r,t\}$, and $\boldsymbol{\varphi}_{\mathrm{RIS}}^{U,e} = \left[\sqrt{\beta_1^{U,e}}e^{j\theta_1^{U,e}}, \sqrt{\beta_2^{U,e}}e^{j\theta_2^{U,e}}, ..., \sqrt{\beta_M^{U,e}}e^{j\theta_M^{U,e}}\right]$. $\theta_m^{U,e}$ and $\beta_m^{U,e}$ are the phase shift and amplitude for the m-th element of STAR-RIS, with $\theta_m^{U,e}\in[0,2\pi)$ and $\beta_m^{U,e}\in[0,\beta_{\max}]$, $\forall m\in\mathcal{M}=\{1,2,...,M\}$. The uplink channels adopt the same model as the downlink channels. Thereby, the uplink channels from user i to the STAR-RIS and that from STAR-RIS to the AP are given by $\mathbf{h}_{i,RIS}^U\in\mathbb{C}^{M\times 1}$ and $\mathbf{h}_{\mathrm{RIS,AP}}^U\in\mathbb{C}^{1\times M}$, respectively. Denote the transmitted signal from user i to the AP as z_i. The signal reflected/transmitted and amplified by the STAR-RIS can be expressed as $z_{\mathrm{RIS}}^U = \mathbf{u}_{\mathrm{RIS}}^{U,e}\left(\sum_{i=1}^I \mathbf{h}_{i,\mathrm{RIS}}^U z_i + n_{\mathrm{RIS}}\right)$. Then the signal received by the AP is $y_{\mathrm{AP}}^U = \mathbf{h}_{\mathrm{RIS,AP}}^U z_{\mathrm{RIS}}^U + n_{\mathrm{AP}}$, where n_{AP} is the noise at the AP.

The power-domain NOMA is applied to leverage its high spectrum efficiency during task offloading, and a two-user NOMA group configuration is employed as outlined in [36]. The total bandwidth is divided into K sub-channels, with $2K=I$. If channel k is allocated to user i, $\delta_{i,k}=1$. Otherwise, $\delta_{i,k}=0$. Thus, we have $\sum_{i=1}^I\delta_{i,k}=I_k$, and $\sum_{k=1}^K I_k = I$. After receiving all users' signals, the AP will decode the superimposed signals based on decoding order $\chi(i,k)$. If $\chi(i,k)>\chi\left(\tilde{i},k\right)$, we have $\pi_{\chi\left(i,\tilde{i},k\right)}=1$. Otherwise, $\pi_{\chi\left(i,\tilde{i},k\right)}=0$. Then, the offloading data rate of user i at channel k can be expressed as

$$L_{i,k}^{\mathrm{off}} = \left(T-\tau\right)B\log\left(1+\frac{\delta_{i,k}p_i\left|\mathbf{h}_{\mathrm{RIS,AP}}^U\mathbf{u}_{\mathrm{RIS}}^{U,e}\mathbf{h}_{i,\mathrm{RIS}}^U\right|^2}{\xi_{i,k}}\right), \quad (6)$$

$$\xi_{i,k} = \sum_{\tilde{i}=1,\tilde{i}\neq i}^I \pi_{\chi\left(i,\tilde{i},k\right)}\delta_{\tilde{i},k}p_{\tilde{i}}\left|\mathbf{h}_{\mathrm{RIS,AP}}^U\mathbf{u}_{\mathrm{RIS}}^{U,e}\mathbf{h}_{i,\mathrm{RIS}}^U\right|^2 + n_{\mathrm{RIS}}^2\left\|\mathbf{h}_{\mathrm{RIS,AP}}^U\mathbf{u}_{\mathrm{RIS}}^{U,e}\right\|^2 + n_{\mathrm{AP}}^2, \quad (7)$$

where B is the bandwidth of each sub-channel. p_i is the transmit power of user i. Thereby, the overall offloading data rata of user i can be given by $L_i^{\mathrm{off}}=\sum_{k=1}^K L_{i,k}^{\mathrm{off}}$.

III. Resource Allocation and Active Beamforming Algorithm Design

In this paper, we aim to maximize the total number of completed task bits for the active STAR-RIS-assisted wireless-powered MEC systems. The total number of completed task bits comprises both the number of offloaded task bits and the number of task bits completed by local computing. Compared to other metrics such as spectral efficiency, the total number of completed task bits can provide a more accurate reflection of the system's computational capability. To achieve the goal of maximizing the total number of completed task bits, the energy transfer time, decoding order, transmit power, CPU frequencies of users, and beamforming of the active STAR-RIS must be jointly optimized.

In the following, we will first focus on the two-user scenario and propose a resource allocation and active beamforming algorithm, which will serve as a foundation for the multiple-user scenarios. To extend the proposed algorithm to multiple-user scenarios, we design a user pairing algorithm for NOMA based on matching theory. Finally, several modifications is implemented to further reduce the complexity of the proposed algorithm for multi-user scenarios.

A. Problem formulation and algorithm design for the two-user scenario

1) Problem formulation: Assume that there are only two users (i.e., user j and user q) in the active STAR-RIS-assisted wireless-powered MEC system, and these two users share the same sub-channel k via NOMA. Subject to the energy consumption constraints, the completed task bits maximization problem for the two-user scenario can be formulated as (P1), as shown at the top of the next page.

In (P1), $\mathbf{z}=\{\mathbf{p},\mathbf{f},\mathbf{u},\tau,\boldsymbol{\pi}\}$. $\mathbf{p}\triangleq\{p_i\}_{i\in\mathcal{I}}$, $\mathbf{f}\triangleq\{f_i\}_{i\in\mathcal{I}}$, $\mathbf{u}\triangleq\left\{\mathbf{u}_{\mathrm{RIS}}^{D,e},\mathbf{u}_{\mathrm{RIS}}^{U,e}\right\}$, and $\pi\triangleq\left\{\pi_{\chi\left(i,\tilde{i},k\right)}\right\}_{i\in\mathcal{I},k\in\mathcal{K}}$. E_{RIS} is the maximum energy budget of STAR-RIS. $P_{\max}$ and $F_{\max}$ are users' maximum transmit power and maximum CPU frequency, respectively. Constraint C1 indicates that the energy consumption of users must be less than their harvested energy. Constraint C2 represents that the energy consumption of active STAR-RIS for signal amplification cannot exceed its maximum energy budget. C3 and C4 represent the phase shift and amplitude constraints of the active STAR-RIS, respectively. C5

$$(\mathrm{P1})\max_{\mathbf{z}}\sum_{i\in\{j,q\}}\left((T-\tau)B\log\left(1+\frac{p_i\left|\mathbf{h}_{\mathrm{RIS,AP}}^{U}\mathbf{u}_{\mathrm{RIS}}^{U,e}\mathbf{h}_{i,\mathrm{RIS}}^{U}\right|^2}{\pi_{\chi(i,\tilde{i},k)}p_{\tilde{i}}\left|\mathbf{h}_{\mathrm{RIS,AP}}^{U}\mathbf{u}_{\mathrm{RIS}}^{U,e}\mathbf{h}_{\tilde{i},\mathrm{RIS}}^{U}\right|^2+n_{\mathrm{RIS}}^2\left\|\mathbf{h}_{\mathrm{RIS,AP}}^{U}\mathbf{u}_{\mathrm{RIS}}^{U,e}\right\|^2+n_{\mathrm{AP}}^2}\right)+\frac{f_i(T-\tau)}{C_i}\right) \tag{8a}$$

$$\text{s.t. C1}:\ (T-\tau)p_i+\kappa(T-\tau)f_i^3\le\tau P_{\mathrm{out},i},\forall i\in\{j,q\}, \tag{8b}$$

$$\text{C2}:\ \tau\sum\nolimits_{e=\{r,t\}}\left(P_{\mathrm{AP}}\left\|\mathbf{u}_{RIS}^{D,e}\mathbf{h}_{\mathrm{AP,RIS}}^{D}\right\|^2+n_{\mathrm{RIS}}^2\left\|\mathbf{u}_{\mathrm{RIS}}^{D,e}\right\|^2\right)+(T-\tau)\left(\sum_{i=1}^{I}\sum\nolimits_{e=\{r,t\}}p_i\left\|\mathbf{u}_{\mathrm{RIS}}^{U,e}\mathbf{h}_{i,\mathrm{RIS}}^{U}\right\|^2+\sum\nolimits_{e=\{r,t\}}n_{\mathrm{RIS}}^2\left\|\mathbf{u}_{\mathrm{RIS}}^{U,e}\right\|^2\right)\le E_{\mathrm{RIS}}, \tag{8c}$$

$$\text{C3}:\ \theta_m^{U/D,e}\in[0,2\pi],\forall m\in\mathcal{M}, \tag{8d}$$

$$\text{C4}:\ \beta_m^{U/D,e}\in[0,\beta_{\max}],\forall m\in\mathcal{M}, \tag{8e}$$

$$\text{C5}:\ 0\le\tau\le T, \tag{8f}$$

$$\text{C6}:\ 0\le p_i\le P_{\max},\forall i\in\{j,q\}, \tag{8g}$$

$$\text{C7}:\ 0\le f_i\le F_{\max},\forall i\in\{j,q\}. \tag{8h}$$

means the energy transfer time should be less than the duration of mission period. C6 and C7 constrain the maximum transmit power and CPU frequency of users.

2) Algorithm design: Problem (P1) is a non-convex optimization problem with highly coupled variables, which is very challenging to solve. Fortunately, in the two-user scenario, there are only two possible decoding orders for the AP. Specifically, if $p_j\left|\mathbf{h}_{\mathrm{RIS,AP}}^{U}\mathbf{u}_{\mathrm{RIS}}^{U,e}\mathbf{h}_{j,\mathrm{RIS}}^{U}\right|^2\ge p_q\left|\mathbf{h}_{\mathrm{RIS,AP}}^{U}\mathbf{u}_{\mathrm{RIS}}^{U,e}\mathbf{h}_{q,\mathrm{RIS}}^{U}\right|^2$, we have $\pi_{\chi(j,q,k)}=1$ and $\pi_{\chi(q,j,k)}=0$. Otherwise, $\pi_{\chi(j,q,k)}=0$ and $\pi_{\chi(q,j,k)}=1$. Therefore, we can separately solve (P1) under these two possible decoding orders.

In order to tackle problem (P1) with pre-given decoding order, we propose an iterative algorithm based on BCD technique [37]. The energy transfer time, transmit power, and beamforming of the active STAR-RIS are updated iteratively until convergence. Unlike the majority of studies employing the BCD algorithm, where optimization variables are obtained after solving a convex optimization problem, we endeavor to derive closed-form solutions for some variables, thereby avoiding the computationally intensive task of repeatedly solving convex optimization problems during each iteration. Next, we will elucidate the detailed processes of solving (P1).

Assuming $\pi_{\chi(j,q,k)}=1$, $\pi_{\chi(q,j,k)}=0$, and with given $\{\mathbf{p},\mathbf{f},\mathbf{u}\}$, we first derive the closed-form solution for the energy transmission time, i.e., τ^*. The derivative of the objective function with respect to τ can be given by

$$\nabla_\tau L=-B\log\left(1+\frac{p_i\left|\mathbf{h}_{\mathrm{RIS,AP}}^{U}\mathbf{u}_{\mathrm{RIS}}^{U,e}\mathbf{h}_{i,\mathrm{RIS}}^{U}\right|^2}{\xi_{i,k}}\right)-\frac{f_i}{C_i}, \tag{9}$$

where $L=L_i^{\mathrm{off}}+L_i^{\mathrm{local}}$. It is clear that the objective function of (P1) is a monotonically decreasing function of τ because $\nabla_\tau L\le 0$ always holds. Therefore, once the range of τ can be determined, we can obtain τ^*.

In (P1), constraints C1, C2, and C5 are related to τ. From C1, we can obtain

$$\frac{Tp_i+\kappa Tf_i^3}{p_i+\kappa f_i^3+P_{\mathrm{out},i}}\le\tau. \tag{10}$$

As for C2, we first define

$$\alpha=\frac{\sum_{e=\{r,t\}}\left(P_{\mathrm{AP}}\left\|\mathbf{u}_{\mathrm{RIS}}^{D,e}\mathbf{h}_{\mathrm{AP,RIS}}^{D}\right\|^2+n_{\mathrm{RIS}}^2\left\|\mathbf{u}_{\mathrm{RIS}}^{D,e}\right\|^2\right)}{\sum_{i=1}^{I}\sum_{e=\{r,t\}}p_i\left\|\mathbf{u}_{\mathrm{RIS}}^{U,e}\mathbf{h}_{i,\mathrm{RIS}}^{U}\right\|^2+\sum_{e=\{r,t\}}n_{\mathrm{RIS}}^2\left\|\mathbf{u}_{\mathrm{RIS}}^{U,e}\right\|^2}. \tag{11}$$

α represents the ratio of the amplification power of the active STAR-RIS for uplink and downlink signals. If $\alpha\ge 1$, the amplification power of the STAR-RIS for AP's energy-carrying signal is greater than that for users' task offloading signals. In this case, from C2, we can obtain an upper bound of τ, which is shown in (12). Hence, the optimal energy transfer time is determined by the lower bound derived from C1, i.e., $\frac{Tp_i+\kappa Tf_i^3}{p_i+\kappa f_i^3+P_{\mathrm{out},i}}$. If $\alpha<1$, the optimal energy transfer time should be the smaller value among the lower bounds given by C1 and C2. Therefore, the optimal energy transfer time τ^* can be obtained as (13).

With τ^* and given $\{\mathbf{p},\mathbf{u}\}$, before deriving the closed-form solution for CPU frequencies of users, we have the following Theorem.

Theorem 1. *When the optimal solution to problem (P1) is obtained, one of constraints C1 and C7 must hold with equality.*

Proof. See Appendix A. □

According to Theorem 1, the optimal CPU frequency of users for local computing can be derived as

$$f_i{}^*=\min\left\{F_{\max},\sqrt[3]{\frac{\tau P_{\mathrm{out},i}-(T-\tau)p_i}{\kappa(T-\tau)}}\right\}. \tag{14}$$

Then, with τ^*, $f_i{}^*$, and given $\{\mathbf{u}\}$, problem (P1) can be

$$\tau \leq \frac{E_{\mathrm{RIS}} - T\left(\sum_{i=1}^{I}\sum_{e=\{r,t\}} p_i\left\|\mathbf{u}_{\mathrm{RIS}}^{U,e}\mathbf{h}_{i,\mathrm{RIS}}^{U}\right\|^2 + \sum_{e=\{r,t\}} n_{\mathrm{RIS}}^2\left\|\mathbf{u}_{\mathrm{RIS}}^{U,e}\right\|^2\right)}{\sum_{e=\{r,t\}}\left(P_{\mathrm{AP}}\left\|\mathbf{u}_{\mathrm{RIS}}^{D,e}\mathbf{h}_{\mathrm{AP,RIS}}^{D}\right\|^2 + n_{\mathrm{RIS}}^2\left\|\mathbf{u}_{\mathrm{RIS}}^{D,e}\right\|^2\right) - \left(\sum_{i=1}^{I}\sum_{e=\{r,t\}} p_i\left\|\mathbf{u}_{\mathrm{RIS}}^{U,e}\mathbf{h}_{i,\mathrm{RIS}}^{U}\right\|^2 + \sum_{e=\{r,t\}} n_{\mathrm{RIS}}^2\left\|\mathbf{u}_{\mathrm{RIS}}^{U,e}\right\|^2\right)} \tag{12}$$

$$\tau^* = \begin{cases} \min\limits_i \frac{Tp_i+\kappa T f_i^3}{p_i+\kappa f_i^3+P_{\mathrm{out},i}}, \alpha \geq 1 \\ \min\limits_i \left\{ \frac{Tp_i+\kappa T f_i^3}{p_i+\kappa f_i^3+P_{\mathrm{out},i}}, \frac{E_{\mathrm{RIS}}-T\left(\sum_{i=1}^{I}\sum_{e=\{r,t\}} p_i\left\|\mathbf{u}_{\mathrm{RIS}}^{U,e}\mathbf{h}_{i,\mathrm{RIS}}^{U}\right\|^2+\sum_{e=\{r,t\}} n_{\mathrm{RIS}}^2\left\|\mathbf{u}_{\mathrm{RIS}}^{U,e}\right\|^2\right)}{\sum\limits_{e=\{r,t\}}\left(P_{\mathrm{AP}}\left\|\mathbf{u}_{\mathrm{RIS}}^{D,e}\mathbf{h}_{\mathrm{AP,RIS}}^{D}\right\|^2+n_{\mathrm{RIS}}^2\left\|\mathbf{u}_{\mathrm{RIS}}^{D,e}\right\|^2\right)-\left(\sum\limits_{i=1}^{I}\sum\limits_{e=\{r,t\}} p_i\left\|\mathbf{u}_{\mathrm{RIS}}^{U,e}\mathbf{h}_{i,\mathrm{RIS}}^{U}\right\|^2+\sum\limits_{e=\{r,t\}} n_{\mathrm{RIS}}^2\left\|\mathbf{u}_{\mathrm{RIS}}^{U,e}\right\|^2\right)} \right\}, \alpha < 1 \end{cases} \tag{13}$$

$$\begin{aligned} (\mathrm{P3}) \max_{\boldsymbol{\gamma},\mathbf{y},\mathbf{p}} & \sum_{i=\{j,q\}}\left(\omega\log\left(1+\gamma_i\right)-\omega\gamma_i+2y_i\sqrt{\left(1+\gamma_i\right)\omega p_i\left|\mathbf{h}_{\mathrm{RIS,AP}}^{U}\mathbf{u}_{\mathrm{RIS}}^{U,e}\mathbf{h}_{i,\mathrm{RIS}}^{U}\right|^2}\right) \\ & - y_j^2\left(p_j\left|\mathbf{h}_{\mathrm{RIS,AP}}^{U}\mathbf{u}_{\mathrm{RIS}}^{U,e}\mathbf{h}_{j,\mathrm{RIS}}^{U}\right|^2+\xi_q\right)-y_q^2\left(p_q\left|\mathbf{h}_{\mathrm{RIS,AP}}^{U}\mathbf{u}_{\mathrm{RIS}}^{U,e}\mathbf{h}_{q,\mathrm{RIS}}^{U}\right|^2+n_{\mathrm{RIS}}^2\left\|\mathbf{h}_{\mathrm{RIS,AP}}^{U}\mathbf{u}_{\mathrm{RIS}}^{U,e}\right\|^2+n_{\mathrm{AP}}^2\right) \quad (16a) \\ & \text{s.t. C1, C2, C6, (15c).} \quad (16b) \end{aligned}$$

$$\begin{aligned} p_j^* &= \min\left\{p_{j,\max}, \frac{\tau P_{\mathrm{out},j}-\kappa(T-\tau)f_j^3}{(T-\tau)}, \frac{y_j^2(1+\gamma_j)\omega\left|\mathbf{h}_{RIS,AP}^{U}\mathbf{u}_{\mathrm{RIS}}^{U,e}\mathbf{h}_{j,\mathrm{RIS}}^{U}\right|^2}{\left(y_j^2\left|\mathbf{h}_{\mathrm{RIS,AP}}^{U}\mathbf{u}_{\mathrm{RIS}}^{U,e}\mathbf{h}_{j,\mathrm{RIS}}^{U}\right|^2-\eta\sum_{e=\{r,t\}}\left\|\mathbf{u}_{\mathrm{RIS}}^{U,e}\mathbf{h}_{j,\mathrm{RIS}}^{U}\right\|^2\right)^2}\right\} \\ p_q^* &= \min\left\{p_{q,\max}, \frac{\tau P_{\mathrm{out},q}-\kappa(T-\tau)f_q^3}{(T-\tau)}, \frac{y_q^2(1+\gamma_q)\omega\left|\mathbf{h}_{\mathrm{RIS,AP}}^{U}\mathbf{u}_{\mathrm{RIS}}^{U,e}\mathbf{h}_{q,\mathrm{RIS}}^{U}\right|^2}{\left(y_q^2\left|\mathbf{h}_{\mathrm{RIS,AP}}^{U}\mathbf{u}_{\mathrm{RIS}}^{U,e}\mathbf{h}_{q,\mathrm{RIS}}^{U}\right|^2-\eta\sum_{e=\{r,t\}}\left\|\mathbf{u}_{\mathrm{RIS}}^{U,e}\mathbf{h}_{q,\mathrm{RIS}}^{U}\right\|^2\right)^2}, \frac{p_j\left|\mathbf{h}_{\mathrm{RIS,AP}}^{U}\mathbf{u}_{\mathrm{RIS}}^{U,e}\mathbf{h}_{j,\mathrm{RIS}}^{U}\right|^2}{\left|\mathbf{h}_{\mathrm{RIS,AP}}^{U}\mathbf{u}_{\mathrm{RIS}}^{U,e}\mathbf{h}_{q,\mathrm{RIS}}^{U}\right|^2}\right\} \end{aligned} \tag{17}$$

reformulated as

$$\begin{aligned} (\mathrm{P2}) \max_{p_j,p_q} & \left(T-\tau\right)B\log\left(1+\frac{p_j\left|\mathbf{h}_{\mathrm{RIS,AP}}^{U}\mathbf{u}_{\mathrm{RIS}}^{U,e}\mathbf{h}_{j,\mathrm{RIS}}^{U}\right|^2}{\xi_q}\right) \\ & +\left(T-\tau\right)B\log\left(1+\frac{p_q\left|\mathbf{h}_{\mathrm{RIS,AP}}^{U}\mathbf{u}_{\mathrm{RIS}}^{U,e}\mathbf{h}_{q,\mathrm{RIS}}^{U}\right|^2}{n_{\mathrm{RIS}}^2\left\|\mathbf{h}_{\mathrm{RIS,AP}}^{U}\mathbf{u}_{\mathrm{RIS}}^{U,e}\right\|^2+n_{\mathrm{AP}}^2}\right) \quad (15a) \\ & \text{s.t.C1, C2, C6,} \quad (15b) \\ & p_j\left|\mathbf{h}_{\mathrm{RIS,AP}}^{U}\mathbf{u}_{\mathrm{RIS}}^{U,e}\mathbf{h}_{j,\mathrm{RIS}}^{U}\right|^2 \geq p_q\left|\mathbf{h}_{\mathrm{RIS,AP}}^{U}\mathbf{u}_{\mathrm{RIS}}^{U,e}\mathbf{h}_{q,\mathrm{RIS}}^{U}\right|^2, \quad (15c) \end{aligned}$$

where $\xi_q = p_q\left|\mathbf{h}_{\mathrm{RIS,AP}}^{U}\mathbf{u}_{\mathrm{RIS}}^{U,e}\mathbf{h}_{q,\mathrm{RIS}}^{U}\right|^2 + n_{\mathrm{RIS}}^2\left\|\mathbf{h}_{\mathrm{RIS,AP}}^{U}\mathbf{u}_{\mathrm{RIS}}^{U,e}\right\|^2 + n_{\mathrm{AP}}^2$. Problem (P2) is also non-convex. To tackle this problem, we first apply the quadratic transform to reformulate (P2) as a convex problem and then utilize Lagrangian dual method to obtain the closed-form expression for users' transmit power.

By introducing auxiliary variables $\boldsymbol{\gamma} = \{\gamma_j, \gamma_q\}$, $\mathbf{y} = \{y_j, y_q\}$, and defining $\omega = (T-\tau)B$, problem (P2) can be transformed into (P3), given at the top of this page.

Theorem 2. *Problem (P2) is equivalent to (P3), i.e., the solution to (P2) is also the solution to (P3), and the optimal objective value of (P2) is equal to that of (P3).*

Proof. See Appendix B. □

Theorem 3. *For Problem (P3) with fixed $\boldsymbol{\gamma}$ and $\mathbf{y}$, the closed-form expression of transmit power can be given by (17), where η is the Lagrangian dual variable for constraint C2.*

Proof. See Appendix C. □

Based on Theorem 2 and Theorem 3, an iterative algorithm can be proposed to obtain the optimal transmit power of users through closed-form updates. The Lagrangian dual variable η is updated by sub-gradient method [38], i.e.,

$$\eta = \left[\eta + \sigma\left(\Psi - E_{\mathrm{RIS}}\right)\right]^+, \tag{18}$$

where $[x]^+ = \max\{x, 0\}$, and σ is the step-size. Ψ is the left-hand-side of C2. The proposed transmit power optimization algorithm for the two-user scenario can be summarized as **Algorithm 1**.

Finally, in order to optimize the beamforming of STAR-RIS, with the obtained optimal τ^*, ${f_i}^*$, and ${p_i}^*$, problem (P1) can be reformulated as (P4) by adopting a similar transformation to (P3), where $\boldsymbol{\gamma}^{\mathrm{RIS}}$ and $\mathbf{y}^{\mathrm{RIS}}$ are auxiliary variables.

For (P4) with fixed $\boldsymbol{\gamma}^{\mathrm{RIS}}$ and $\mathbf{y}^{\mathrm{RIS}}$, it is still non-convex due to constraints C1 and (15c). We first exploit the first-order Taylor expansion to the right-of-hand of C1 at the l-th iteration, i.e.,

$$\begin{aligned} & \tau P_{\mathrm{out},i} \geq \tau P_{\mathrm{out},i}\big|_{\mathbf{u}_{\mathrm{RIS}}^{D,e}=\left(\mathbf{u}_{\mathrm{RIS}}^{D,e}\right)^{(l)}} \\ & +\tau\nabla_{\mathbf{u}_{\mathrm{RIS}}^{D,e}=\left(\mathbf{u}_{\mathrm{RIS}}^{D,e}\right)^{(l)}} P_{\mathrm{out},i}\left(\mathbf{u}_{\mathrm{RIS}}^{D,e}-\left(\mathbf{u}_{\mathrm{RIS}}^{D,e}\right)^{(l)}\right). \end{aligned} \tag{20}$$

For ease of representation, the right-hand side of the above

$$
\begin{aligned}
(\mathrm{P4}) \max_{\mathbf{u}_{\mathrm{RIS}}^{U,e},\mathbf{u}_{\mathrm{RIS}}^{D,e},\boldsymbol{\gamma}^{\mathrm{RIS}},\mathbf{y}^{\mathrm{RIS}}} \Omega = & \sum\nolimits_{i\in\{q,j\}} \left(\log\left(1+\gamma_i^{\mathrm{RIS}}\right)-\gamma_i^{\mathrm{RIS}}\right) \\
& + \sum\nolimits_{i\in\{q,j\}} 2y_i^{\mathrm{RIS}}\sqrt{\left(1+\gamma_i^{\mathrm{RIS}}\right)p_i}\mathrm{Re}\left(\mathbf{h}_{\mathrm{RIS,AP}}^{U}\mathbf{u}_{\mathrm{RIS}}^{U,e}\mathbf{h}_{i,\mathrm{RIS}}^{U}\right) \\
& - \left(y_j^{\mathrm{RIS}}\right)^2\left(p_j\left|\mathbf{h}_{\mathrm{RIS,AP}}^{U}\mathbf{u}_{\mathrm{RIS}}^{U,e}\mathbf{h}_{j,\mathrm{RIS}}^{U}\right|^2+p_q\left|\mathbf{h}_{\mathrm{RIS,AP}}^{U}\mathbf{u}_{\mathrm{RIS}}^{U,e}\mathbf{h}_{q,\mathrm{RIS}}^{U}\right|^2+n_{\mathrm{RIS}}^2\left\|\mathbf{h}_{\mathrm{RIS,AP}}^{U}\mathbf{u}_{\mathrm{RIS}}^{U,e}\right\|^2+n_{\mathrm{AP}}^2\right) \\
& - \left(y_q^{\mathrm{RIS}}\right)^2\left(p_q\left|\mathbf{h}_{\mathrm{RIS,AP}}^{U}\mathbf{u}_{\mathrm{RIS}}^{U,e}\mathbf{h}_{q,\mathrm{RIS}}^{U}\right|^2+n_{\mathrm{RIS}}^2\left\|\mathbf{h}_{\mathrm{RIS,AP}}^{U}\mathbf{u}_{\mathrm{RIS}}^{U,e}\right\|^2+n_{\mathrm{AP}}^2\right) \qquad (19a) \\
\text{s.t. } & \mathrm{C1}-\mathrm{C4},(15\mathrm{c})\,. \qquad (19b)
\end{aligned}
$$

Algorithm 1 Users' transmit power optimization algorithm for two-user scenario.

1. Initialize the vectors $\mathbf{p}$, $\mathbf{y}$, $\boldsymbol{\gamma}$, and set the iterative number $l=0$;
2. **while** $\left|G\left(\mathbf{p}^{(l+1)},\boldsymbol{\gamma}^{(l+1)},\mathbf{y}^{(l+1)}\right)-G\left(\mathbf{p}^{(l)},\boldsymbol{\gamma}^{(l)},\mathbf{y}^{(l)}\right)\right|\geq\varepsilon$ **do**
3. Update $\mathbf{y}^{(l)}$ based on (34);
4. Update $\boldsymbol{\gamma}^{(l)}$ based on (33);
5. **repeat**
6. Initialize the dual variable $\eta^{(t)}$ and set $t=0$;
7. Update $\mathbf{p}^{(t)}$ based on (17);
8. Update $\eta^{(t)}$ based on (18);
9. $t=t+1$;
10. **Until** the objective function of (P3) converges
11. Set $\mathbf{p}^{(l)}=\mathbf{p}^{(t)}$;
12. $l=l+1$;
13. **end while**

inequality is denoted as $\Xi\left(\mathbf{u}_{\mathrm{RIS}}^{D,e}\right)$. Then, by replacing the right-hand side of C1 with $\Xi\left(\mathbf{u}_{\mathrm{RIS}}^{D,e}\right)$, C1 can be transformed into a linear constraint. The same technique is adopted for (15c). Thus, we have

$$
\begin{aligned}
& p_j\left|\mathbf{h}_{\mathrm{RIS,AP}}^{U}\mathbf{u}_{\mathrm{RIS}}^{U,e}\mathbf{h}_{j,\mathrm{RIS}}^{U}\right|^2 \geq p_j\left|\mathbf{h}_{\mathrm{RIS,AP}}^{U}\left(\mathbf{u}_{\mathrm{RIS}}^{U,e}\right)^{(l)}\mathbf{h}_{j,\mathrm{RIS}}^{U}\right|^2 \\
& +2p_j\left(\left(\mathbf{u}_{\mathrm{RIS}}^{U,e}\right)^{(l)}\right)^H\Pi\left(\mathbf{u}_{\mathrm{RIS}}^{U,e}-\left(\mathbf{u}_{\mathrm{RIS}}^{U,e}\right)^{(l)}\right),
\end{aligned} \qquad (21)
$$

where $\Pi=\left(\mathbf{h}_{\mathrm{RIS,AP}}^{U}\right)^H\mathbf{h}_{j,\mathrm{RIS}}^{U}\left(\mathbf{h}_{j,\mathrm{RIS}}^{U}\right)^H\mathbf{h}_{\mathrm{RIS,AP}}^{U}$, and the right-hand side of (21) is denoted as $\mathrm{P}\left(\mathbf{u}_{\mathrm{RIS}}^{U,e}\right)$. After the above operations, (P4) can be reformulated as

$$
\begin{aligned}
(\mathrm{P5}) \max_{\mathbf{u}_{\mathrm{RIS}}^{U,e},\mathbf{u}_{\mathrm{RIS}}^{D,e}} & \ \Omega \qquad (22a) \\
\text{s.t. } & \mathrm{C2}-\mathrm{C4}, \qquad (22b) \\
& (T-\tau)\,p_i+\kappa\,(T-\tau)\,f_i^3\leq\Xi\left(\mathbf{u}_{\mathrm{RIS}}^{D,e}\right), \qquad (22c) \\
& \mathrm{P}\left(\mathbf{u}_{\mathrm{RIS}}^{U,e}\right)\geq p_q\left|\mathbf{h}_{\mathrm{RIS,AP}}^{U}\mathbf{u}_{\mathrm{RIS}}^{U,e}\mathbf{h}_{q,\mathrm{RIS}}^{U}\right|^2. \qquad (22d)
\end{aligned}
$$

Problem (P5) is a standard quadratic constraint quadratic programming (QCQP) problem which can be effectively solved by standard convex optimization algorithm. After iteratively updating $\mathbf{u}_{\mathrm{RIS}}^{U,e}$ and $\mathbf{u}_{\mathrm{RIS}}^{D,e}$ by solving (P5) until convergence, we can obtain the optimal solution to (P4) with fixed $\boldsymbol{\gamma}^{\mathrm{RIS}}$ and $\mathbf{y}^{\mathrm{RIS}}$.

According to Theorem 2, the closed-form solutions of $\boldsymbol{\gamma}^{\mathrm{RIS}}$ and $\mathbf{y}^{\mathrm{RIS}}$ can be given by

$$
\begin{aligned}
y_j^{\mathrm{RIS}^*} &= \frac{\omega\left(1+\gamma_j^{\mathrm{RIS}}\right)p_j\left|\mathbf{h}_{\mathrm{RIS,AP}}^{U}\mathbf{u}_{\mathrm{RIS}}^{U,e}\mathbf{h}_{j,\mathrm{RIS}}^{U}\right|^2}{p_j\left|\mathbf{h}_{\mathrm{RIS,AP}}^{U}\mathbf{u}_{\mathrm{RIS}}^{U,e}\mathbf{h}_{j,\mathrm{RIS}}^{U}\right|^2+\xi_q} \\
y_q^{\mathrm{RIS}^*} &= \frac{\omega\left(1+\gamma_q^{\mathrm{RIS}}\right)p_q\left|\mathbf{h}_{\mathrm{RIS,AP}}^{U}\mathbf{u}_{\mathrm{RIS}}^{U,e}\mathbf{h}_{q,\mathrm{RIS}}^{U}\right|^2}{p_q\left|\mathbf{h}_{\mathrm{RIS,AP}}^{U}\mathbf{u}_{\mathrm{RIS}}^{U,e}\mathbf{h}_{q,\mathrm{RIS}}^{U}\right|^2+n_{\mathrm{RIS}}^2\left\|\mathbf{h}_{\mathrm{RIS,AP}}^{U}\mathbf{u}_{\mathrm{RIS}}^{U,e}\right\|^2+n_{\mathrm{AP}}^2}
\end{aligned} \qquad (23)
$$

$$
\begin{aligned}
\gamma_j^{\mathrm{RIS}^*} &= \frac{p_j\left|\mathbf{h}_{\mathrm{RIS,AP}}^{U}\mathbf{u}_{\mathrm{RIS}}^{U,e}\mathbf{h}_{j,\mathrm{RIS}}^{U}\right|^2}{p_q\left|\mathbf{h}_{\mathrm{RIS,AP}}^{U}\mathbf{u}_{\mathrm{RIS}}^{U,e}\mathbf{h}_{q,\mathrm{RIS}}^{U}\right|^2+n_{\mathrm{RIS}}^2\left|\mathbf{h}_{\mathrm{RIS,AP}}^{U}\mathbf{u}_{\mathrm{RIS}}^{U,e}\right|^2+n_{\mathrm{AP}}^2} \\
\gamma_q^{\mathrm{RIS}^*} &= \frac{p_q\left|\mathbf{h}_{\mathrm{RIS,AP}}^{U}\mathbf{u}_{\mathrm{RIS}}^{U,e}\mathbf{h}_{q,\mathrm{RIS}}^{U}\right|^2}{n_{\mathrm{RIS}}^2\left|\mathbf{h}_{\mathrm{RIS,AP}}^{U}\mathbf{u}_{\mathrm{RIS}}^{U,e}\right|^2+n_{\mathrm{AP}}^2}
\end{aligned} \qquad (24)
$$

Then, similar to Algorithm 1, we iteratively update $\mathbf{y}^{\mathrm{RIS}}$, $\boldsymbol{\gamma}^{\mathrm{RIS}}$ and $\mathbf{u}_{\mathrm{RIS}}^{U/D,e}$ until convergence. The active beamforming design for two-user scenario is summarized as **Algorithm 2**. With the optimal active beamforming matrix $\mathbf{u}_{\mathrm{RIS}}^{U/D,e}$, the amplitude and phase shift for each element of active STAR-RIS can be expressed as

$$
\beta_m^{U/D,e}=\left\|\left[\mathbf{u}_{\mathrm{RIS}}^{U/D,e}\right]_{m,m}\right\|_2,\ \theta_m^{U/D,e}=\arg\left(\left[\mathbf{u}_{\mathrm{RIS}}^{U/D,e}\right]_{m,m}\right), \qquad (25)
$$

where $[\cdot]_{m,m}$ represents the (m,m)-th element of matrix.

Define the objective function of (P1) as $F_{(p1)}(n)$, where n represents the index of possible decoding order, i.e.,

$$
n=\begin{cases} 1, & \text{if } \pi_{\chi(j,q,k)}=1 \text{ and } \pi_{\chi(q,j,k)}=0; \\ 2, & \text{if } \pi_{\chi(j,q,k)}=0 \text{ and } \pi_{\chi(q,j,k)}=1. \end{cases} \qquad (26)
$$

Based on the above solutions to τ^*, ${f_i}^*$, ${p_i}^*$ and $\mathbf{u}_{\mathrm{RIS}}^{U/D,e^*}$, the proposed algorithm for solving problem (P1) is summarized in **Algorithm 3**.

3) Discussion: It can be noted that (P1) is first decomposed into two problems according to the possible decoding orders. For each problem, an iterative algorithm is proposed to obtain the optimal solutions for energy transfer time, CPU frequency, transmit power, and active beamforming. Therefore, the computational complexity of the proposed Algorithm 3 mainly depends on the number of iterations in the inner loop and the complexity of Algorithms 1 and 2. Algorithm 1 has linear computational complexity since it only executes closed-form updates. Thus, the computational complexity of Algorithm 1 can be given by $\mathcal{O}_1\left(L_1L_2\right)$, where L_1 and L_2 are the iteration numbers of Algorithm 1 for the outer loop and inner loop, respectively. For Algorithm 2, besides the closed-form

Algorithm 2 Active beamforming design for two-user scenario.

1. Initialize the vectors $\mathbf{u}_{\mathrm{RIS}}^{U,e}, \mathbf{u}_{\mathrm{RIS}}^{D,e}, \boldsymbol{\gamma}^{\mathrm{RIS}}, \mathbf{y}^{\mathrm{RIS}}$, and set the iterative number $l=0$;
2. **while** $\left|\Omega\left(\mathbf{u}_{\mathrm{RIS}}^{U,e}, \mathbf{u}_{\mathrm{RIS}}^{D,e}, \gamma^{\mathrm{RIS}}, \mathbf{y}^{\mathrm{RIS}}\right)^{(l+1)} - \Omega\left(\mathbf{u}_{\mathrm{RIS}}^{U,e}, \mathbf{u}_{\mathrm{RIS}}^{D,e}, \boldsymbol{\gamma}^{\mathrm{RIS}}, \mathbf{y}^{\mathrm{RIS}}\right)^{(l)}\right| \geq \varepsilon$ **do**
3. Update $\left(\mathbf{y}^{\mathrm{RIS}}\right)^{(l)}$ based on (23);
4. Update $\left(\boldsymbol{\gamma}^{\mathrm{RIS}}\right)^{(l)}$ based on (24);
5. **repeat**
6. Initialize the iterative index $t=0$;
7. Calculate $\Xi\left(\mathbf{u}_{\mathrm{RIS}}^{D,e}\right)$ and $\mathrm{P}\left(\mathbf{u}_{\mathrm{RIS}}^{U,e}\right)$ based on (20) and (21), respectively;
8. Solve the QCQP problem (P5) to obtain $\left(\mathbf{u}_{\mathrm{RIS}}^{U,e}\right)^{(t)}, \left(\mathbf{u}_{\mathrm{RIS}}^{D,e}\right)^{(t)}$;
9. Update the iterative index t;
10. **Until** the objective function of (P5) converges;
11. Set $\left(\mathbf{u}_{\mathrm{RIS}}^{U/D,e}\right)^{(l)} = \left(\mathbf{u}_{\mathrm{RIS}}^{U/D,e}\right)^{(t)}$;
12. $l = l+1$;
13. **end while**

Algorithm 3 Resource allocation and active beamforming algorithm (RAABA) for two-user scenario.

1. Set the index number for decoding order as $n=1$;
2. **while** $n \leq 2$ **do**
3. Initialize $\mathbf{p}, \mathbf{f}, \mathbf{u}_{\mathrm{RIS}}^{D/U}, \tau$, and set $l=0$;
4. **repeat**
5. Calculate α based on (11);
6. Update $\tau^{(l)}$ based on (13);
7. Update $\mathbf{f}^{(l)}$ based on (14);
8. Update $\mathbf{p}^{(l)}$ based on Algorithm 1;
9. Update $\mathbf{u}^{(l)}$ based on Algorithm 2;
10. Update the iterative index $l = l+1$;
11. **until** the objective function of (P1) converges;
12. $n = n+1$;
13. **end while**
14. **Output** $\boldsymbol{\pi}^* = \arg\max F_{(p1)}(n)$ and the corresponding $\mathbf{p}, \mathbf{f}, \mathbf{u}_{\mathrm{RIS}}^{U/D}, \tau$.

updating, it involves a sequence of QCQP problems which can be solved using semi-definite programming (SDP). Hence, the computational complexity of Algorithm 2 can be expressed as $\mathcal{O}_2\left(L_3 L_4 (4M)^{3.5}\right)$, where L_3 and L_4 are iteration numbers for the outer loop and inner loop of Algorithm 2 [24]. With $\mathcal{O}_1$ and $\mathcal{O}_2$, and denoting the iteration number for inner loop of Algorithm 3 as L_5, the overall computational complexity of Algorithm 3 can be given by $\mathcal{O}\left(2L_5\left(\mathcal{O}_1+\mathcal{O}_2\right)\right)$, which is in polynomial complexity.

Algorithm 3 executes the inner loop twice. For each iteration of the inner loop, we have

$$\begin{aligned} F\left(\tau^{(l)}, \mathbf{f}^{(l)}, \mathbf{p}^{(l)}, \mathbf{u}^{(l)}\right) &\overset{(1)}{\leq} F\left(\tau^{(l+1)}, \mathbf{f}^{(l)}, \mathbf{p}^{(l)}, \mathbf{u}^{(l)}\right) \\ &\overset{(2)}{\leq} F(\tau^{(l+1)}, \mathbf{f}^{(l+1)}, \mathbf{p}^{(l)}, \mathbf{u}^{(l)}) \overset{(3)}{\leq} F(\tau^{(l+1)}, \mathbf{f}^{(l+1)}, \mathbf{p}^{(l+1)}, \mathbf{u}^{(l)}) \\ &\overset{(4)}{\leq} F\left(\tau^{(l+1)}, \mathbf{f}^{(l+1)}, \mathbf{p}^{(l+1)}, \mathbf{u}^{(l+1)}\right). \end{aligned} \tag{27}$$

The inequalities (1)-(3) hold because $\tau^{(l+1)}$, $\mathbf{f}^{(l+1)}$, and $\mathbf{p}^{(l+1)}$ are optimal solutions to (P1) when all other variables are fixed. The inequality (4) follows from the fact that Algorithm 2 outputs $\mathbf{u}^{(l+1)}$ and guarantees the objective function non-decreasing. Thus, the objective function of problem (P1) with a given decoding order gradually increases after each iteration. In addition, since the total number of completed task bits is upper-bounded, the objective function must converge after a limited number of iterations.

B. Problem formulation and algorithm design for multi-user scenarios

For practical active STAR-RIS-assisted wireless-powered MEC systems, it is inevitable to support more than two users. Therefore, building upon the solution for the two-user scenario, we now formulate the completed task bits maximization problem for multi-user scenarios.

1) Problem formulation: When there are multiple users in active STAR-RIS-assisted wireless-powered MEC systems, constraints C2-C5 in problem (P1) remain effective, while constrains C1, C6, and C7 need to be modified to apply to all users in $\mathcal{I}$. Besides, the channel allocation indicator $\delta_{i,k}$ is required to be taken into consideration. Thus, the completed task bits maximization problem for multi-user scenarios can be formulated as

$$(\mathrm{P6}) \max_{\mathbf{z}_m} \sum_{i=1}^{I} \left(L_i^{\mathrm{off}} + L_i^{\mathrm{local}}\right) \tag{28a}$$

$$\text{s.t. } \mathrm{C2}, \mathrm{C3}, \mathrm{C4}, \mathrm{C5}, \tag{28b}$$

$$(T-\tau)\, p_i + \kappa\,(T-\tau)\, f_i^3 \leq \tau P_{\mathrm{out},i}, \forall i \in \mathcal{I}, \tag{28c}$$

$$0 \leq p_i \leq P_{\max}, \forall i \in \mathcal{I}, \tag{28d}$$

$$0 \leq f_i \leq F_{\max}, \forall i \in \mathcal{I}, \tag{28e}$$

$$\sum_{i=1}^{I} \delta_{i,k} = 2, \forall k \in \mathcal{K}, \tag{28f}$$

$$\sum_{k=1}^{K} \delta_{i,k} = 1, \forall i \in \mathcal{I}, \tag{28g}$$

$$\delta_{i,k} \in \{0,1\}, \forall i \in \mathcal{I}, k \in \mathcal{K}, \tag{28h}$$

where $\mathbf{z}_m = \{\mathbf{p}, \mathbf{f}, \mathbf{u}, \tau, \boldsymbol{\pi}, \boldsymbol{\delta}\}$. $\boldsymbol{\delta} \triangleq \{\delta_{i,k}\}_{i\in\mathcal{I}, k\in\mathcal{K}}$. Constraint (28f) represents each channel can be allocated to at most two users. (28g) indicates that each user can only occupy one channel.

2) Algorithm design: Compared to the two-user scenario, it is more challenging to obtain the resource allocation and active beamforming solutions for problem (P6). This is because, in addition to the joint optimization of energy transfer time, transmit power, CPU frequency, and beamforming of active STAR-RIS, we must also determine which users should be

paired to share the same channel when offloading task bits to the AP. However, the user pairing problem for NOMA is NP-hard [39]. To solve problem (P6), we first propose a user pairing algorithm based on matching theory, and then extend Algorithm 3 to solve (P6) with the optimized user pairing strategy. Before introducing the user pairing algorithm, we need to define the matching function, swap matching, and the swap-blocking pair.

Definition 1: In the proposed matching model, E is defined as a matching function satisfying: (1) $|\mathrm{E}(i)|=1, \forall i \in \mathcal{I}$; (2) $|\mathrm{E}(k)|=2, \forall k \in \mathcal{K}$; (3) $\mathrm{E}(i)=k$ if and only if $i \in \mathrm{E}(k)$. Conditions (1) and (2) correspond to constraints (28f) and (28g) in (P6). Condition (3) indicates that if user i is matched with channel k, channel k is also matched with user i.

Definition 2: A swap matching is defined as [40]–[42]

$$\mathrm{E}_i^j = \left\{\mathrm{E} \backslash \left\{(i, \mathrm{E}(i)),(j, \mathrm{E}(j))\right\} \cup \left\{(i, \mathrm{E}(j)),(j, \mathrm{E}(i))\right\}, \right. \tag{29}$$

which means user i and user j switch their offloading channels, while the other users maintain their current channels.

Definition 3: For a matching model with matching function E, (i, j) is a swap-blocking pair if and only if

$$\begin{aligned} &\forall n \in \{i, j, \mathrm{E}(i), \mathrm{E}(j)\}, U_n\left(\mathrm{E}_i^j\right) \geq U_n(\mathrm{E}), \\ &\exists n \in \{i, j, \mathrm{E}(i), \mathrm{E}(j)\}, U_n\left(\mathrm{E}_i^j\right) > U_n(\mathrm{E}), \end{aligned} \tag{30}$$

where $U_n\left(\mathrm{E}_i^j\right)$ and $U_n(\mathrm{E})$ are utility functions of n under matching function E_i^j and E, respectively. For user n, the utility is its offloading data rate under corresponding matching function, i.e, $U_n\left(\mathrm{E}_i^j\right)=L_{n, \mathrm{E}_i^j(n)}^{\mathrm{off}}$, and $U_n(\mathrm{E})=L_{n, \mathrm{E}(n)}^{\mathrm{off}}$. For channel n, the utility refers to the sum of offloading data rates for all users that are allocated to channel n. Thus, we have $U_n\left(\mathrm{E}_i^j\right)=\sum_{\mathrm{E}_i^j(n)} L_{\mathrm{E}_i^j(n), n}^{\mathrm{off}}$, and $U_n(\mathrm{E})=\sum_{\mathrm{E}(n)} L_{\mathrm{E}(n), n}^{\mathrm{off}}$.

With the above definitions, the proposed matching-theory-based user pairing algorithm is summarized as **Algorithm 4**. Algorithm 4 begins with Initialization (Steps 1-15), and then executes the Swapping Process (Steps 16-21) until there is no swap-blocking pair.

i) Initialization: Denote the sets of users allocated to channel k, proposed to channel k, and rejected by channel k as N_k^A, N_k^P, and N_k^R, respectively. The set of channels rejected by user i is expressed as C_i^R. The set of unmatched users is given by S_{un}. The preference list can be generated by calculating utilities, where the inter-user interference is ignored since each channel has not been allocated to any users. The transmit power of users is initialized as $p_{i,\max}$. The phase shift and amplitude for the m-th element of STAR-RIS are set as $\theta_m^{U,e}=0$ and $\beta_m^{U,e}=\beta_{\max}$. At the end of initialization, all users are allocated to a specific channel.

ii) Swapping Process: To further improve utilities, users will execute swap operations, where the swap among a swap-blocking pair ensures an increase in utilities. During this process, the utility is calculated by considering the inter-user interference. Additionally, to prevent flip-flopping in the Swapping Process, we assume that each user i can swap with another user j at most twice. The Swapping Process will end when there are no swap-blocking pairs.

Algorithm 4 Matching-theory based user pairing algorithm.

1. Initialize the preference lists of all users and channels based on their utilities. Set $S_{\mathrm{un}}=\mathcal{I}$, $N_k^P=\emptyset, N_k^R=\emptyset, N_k^A=\emptyset$, and $C_i^R=\emptyset$.
2. **repeat**
3. **for** i in S_{un} **do**
4. User i proposes to the best channel that has never rejected it before, i.e., $k \in \mathcal{K} \backslash C_i^R$ and update N_k^P;
5. **end for**
6. **for** k in $\mathcal{K}$ **do**
7. **if** the number of users in $N_k^P \cup N_k^A \leq 2$ **then**
8. Accept users in N_k^P, and $N_k^A=N_k^A \cup N_k^A$;
9. Remove the matched users from S_{un};
10. **else**
11. Channel k keeps the most preferred 2 users;
12. Update N_k^A, N_k^R, S_{un}, and C_i^R;
13. **end if**
14. **end for**
15. **until** $S_{\mathrm{un}}=\emptyset$
16. **repeat**
17. For user $i \in N_k^A$, search for another user $j \in N_{\tilde{k}}^A$;
18. **if** (i, j) is a swap-blocking pair **then**
18. Update the current matching state to E_i^j;
19. **else**
20. Keep the current matching state;
21. **until** No swap-blocking pair is found.

With Algorithm 4, we can obtain the optimized matching function E, which can be easily mapped into $\delta_{i,k}$. Since each user pair contains two users, we can extend Algorithm 3 to solve (P6) with given $\delta_{i,k}$. Specifically, for the energy transfer time τ, it can still be calculated according to (13), but the difference lies in $i \in \mathcal{I}$. Theorem 1 still holds for the multi-user scenarios. Thus, the optimal CPU frequency of users can be derived by (14). The transmit power of users in each pair can be obtained via Algorithm 1 under a specific decoding order. Finally, by expanding the user set to multiple users, Algorithm 2 can output the active beamforming strategy for problem (P6). Therefore, the proposed resource allocation and active beamforming algorithm for multi-user scenarios, named RAABAM, can be summarized as **Algorithm 5**.

3) Discussion: From Algorithm 5, it can be noted that the user pairing strategy is not updated during the iteration. This is because if the user pairing strategy changes, the structure of problem (P6) will also change, making it impossible to ensure the convergence of the proposed iterative algorithm. Additionally, despite there are $2^{I/2}$ potential decoding orders in the entire system, it is still much smaller than $I!$ in traditional NOMA systems without a user pairing strategy when $I>2$.

The following provides a theoretical analysis of the computational complexity, convergence and optimality of the proposed RAABAM algorithm. Since the iteration part of

Algorithm 5 Resource allocation and active beamforming algorithm for multi-user scenarios (RAABAM).

1. Obtain user pairing strategy via Algorithm 4;
2. Set the index number for decoding order as $n = 1$;
3. **while** $n \leq 2^{I/2}$ **do**
4. Initialize $\mathbf{p}, \mathbf{f}, \mathbf{u}_{\mathrm{RIS}}^{D/U}, \tau$, and set $l = 1$;
5. **repeat**
6. Update $\tau^{(l)}$ based on (13);
7. **for** each user pair **do**
8. Update $\mathbf{f}^{(l)}$ based on (14);
9. Update $\mathbf{p}^{(l)}$ based on Algorithm 1;
10. **end for**
11. Update $\mathbf{u}^{(l)}$ based on Algorithm 2;
12. Update the iterative index $l = l + 1$;
13. **until** the objective function of (P6) converges;
14. $n = n + 1$;
15. **end while**
16. **Output** $\boldsymbol{\pi}^* = \arg\max F_{(p6)}(n)$ and the corresponding $\{\mathbf{p}, \mathbf{f}, \mathbf{u}, \tau, \boldsymbol{\delta}\}$.

RAABAM algorithm is extended from Algorithm 3, its computational complexity and convergence are the same as we discussed in Section III-A 3). For Algorithm 4, given that the numbers of users and channels are limited and the utilities are upper bounded, the number of swap-blocking pairs is limited. Therefore, Algorithm 4 will converge when no more swap operations occur. The computational complexity for initialization of Algorithm 4 mainly depends on the number of user proposals. In the worst case, each user makes a proposal to all channels, and thus the computational complexity for initialization can be expressed as $\mathcal{O}(IK)$. The computational complexity for swapping process is given by $\mathcal{O}\left(I^2\right)$. Thus, the overall computational complexity of user pairing in RAABAM can be expressed as $O\left(I^2 + KI\right)$. When adopting the exhaustive search algorithm to solve user pairing problem, the computational complexity can be expressed as $O\left(I!/2^K\right)$, which grows super-exponentially with the number of users. As the number of users increases, the computational complexity of exhaustive search algorithm becomes intolerable and thus impractical for large-scale systems.

We next analyze the optimality of proposed RAABAM algorithm. The RAABAM algorithm starts by executing Algorithm 4 to obtain the user pairing strategy. The matching-theory-based Algorithm 4 ensures that the obtained user pairing strategy is a stable matching, i.e., no swap-blocking pair exists in the system. Although Algorithm 4 cannot obtain the globally optimal solution, it improves the utility through a finite number of swaps. With obtained user pairing strategy, the RAABAM algorithm performs an exhaustive search over all possible decoding orders in the outer loop to achieve the globally optimal decoding order. For each decoding order, the inner loop of RAABAM algorithm adopts an alternating optimization approach to iteratively update the resource allocation and beamforming. The inner loop of RAABAM algorithm is a typical BCD algorithm, and it can achieve the local optimal solution with a fast convergence speed. Therefore, based on above analysis, our proposed RAABAM algorithm can achieve the suboptimal solution to the completed task bits maximization problem for multi-user scenarios.

4) Lower-complexity algorithm design: When solving problem (P1) with two users, we find that if one user is located at the reflection space and the other one is located at the transmission space, the noise amplified by active STAR-RIS has different impacts on these two users, which complicates the optimization of users' transmit power. In addition, due to the coupling relationships of the two users' transmit power in constraint C2 and the objective function, we adopt the quadratic transform and design Algorithm 1 to tackle the transmit power optimization iteratively. However, we notice that if these two users are located at the same side of STAR-RIS, they experience identical noise amplified by the active STAR-RIS. Thus, we have the following Theorem 4.

Theorem 4. *When two users (i.e., users i and j) occupying the same channel are located at the same side of STAR-RIS, and the energy budget of STAR-RIS is sufficient, the optimal transmit power of these two users in problem (P2) can be given by*

$$\begin{aligned} p_j^* &= \min\left\{p_{j,\max}, \tfrac{\tau P_{\mathrm{out},j} - \kappa(T-\tau) f_j^3}{(T-\tau)}\right\} \\ p_q^* &= \min\left\{p_{q,\max}, \tfrac{\tau P_{\mathrm{out},q} - \kappa(T-\tau) f_q^3}{(T-\tau)}, \tfrac{p_j \left|\mathbf{h}_{\mathrm{RIS,AP}}^U \mathbf{u}_{\mathrm{RIS}}^{U,e} \mathbf{h}_{j,\mathrm{RIS}}^U\right|^2}{\left|\mathbf{h}_{\mathrm{RIS,AP}}^U \mathbf{u}_{\mathrm{RIS}}^{U,e} \mathbf{h}_{q,\mathrm{RIS}}^U\right|^2}\right\}. \end{aligned} \tag{31}$$

Proof. See Appendix D. □

The above findings, along with Theorem 4, provide valuable insights into reducing the complexity of the proposed RAABAM (Algorithm 5). The low-complexity resource allocation and active beamforming algorithm, named L-RAABAM, is summarized as **Algorithm 6**.

In L-RAABAM algorithm, when initializing $\mathbf{p}, \mathbf{f}, \mathbf{u}$ and τ, we can set the amplitude and phase shift of each element in active STAR-RIS's beamforming matrix $\mathbf{u}^{(0)}$ as $\left(\beta_m^{U/D,e}\right)^{(0)} = 0.5$ and $\left(\theta_m^{U/D,e}\right)^{(0)} = 0$, respectively. The the energy transfer time is initialized as $\tau^{(0)} = \frac{T}{2}$. The initial transmit power and CPU frequency of user i can be set as $p_i^{(0)} = \frac{\tau^{(0)} P_{\mathrm{out},i}}{2\left(T-\tau^{(0)}\right)}$ and $f_i^{(0)} = \sqrt[3]{\frac{\tau^{(0)} P_{\mathrm{out},i}}{2\kappa\left(T-\tau^{(0)}\right)}}$, respectively. It can be found that the initial point of $\mathbf{p}, \mathbf{f}, \mathbf{u}$ and τ can satisfy all constraints of problem (P6). Then, by iteratively updating $\mathbf{p}, \mathbf{f}, \mathbf{u}$ and τ until convergence, we can obtain the suboptimal solution to problem (P6) under the given user pairing strategy and decoding order.

The diagrams of RAABAM and L-RAABAM are illustrated in Fig. 2. From Fig. 2, it can be seen that different from RAABAM, the L-RAABAM algorithm in Fig. 2 (b) executes Algorithm 4 separately for both reflection and transmission spaces, which ensures that any specific user can be paired with another one located at the same side of the STAR-RIS. Since the number of users and channels in reflection and transmission spaces is half of the full space, the computational complexity of user pairing in L-RAABAM can be given by $\mathcal{O}\left(\left(I^2 + KI\right)/2\right)$. It can be found that the computational complexity of user pairing can be significantly

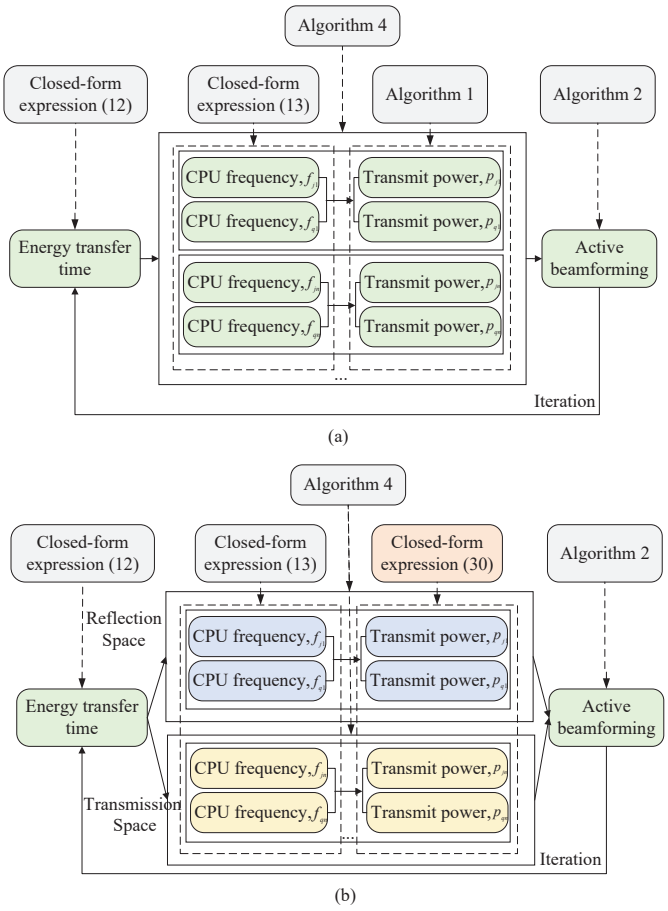

Fig. 2. (a) The diagram of Algorithm 5; (b) The diagram of Algorithm 6.

reduced by executing Algorithm 4 separately in the reflection and transmission spaces. Meanwhile, during the iteration of L-RAABAM, the transmit power of users can be directly updated by a closed-form expression rather than by executing Algorithm 1, which also effectively reduces the complexity of transmit power optimization.

IV. Simulation Results

In this section, we present simulation results to evaluate the performance of the proposed algorithms for the active STAR-RIS-assisted wireless-powered MEC. The considered simulation setup is shown in Fig. 3, where a Cartesian coordinate system is established with O as the origin. The AP is located at $(0, 3, 0)$. The users are distributed in a circular area with a radius of 2 meters centered at $(10, 0, 0)$. The STAR-RIS is deployed on the $x-z$ plane, where both the y and z coordinates of the STAR-RIS are 0. The bandwidth for each subchannel is 1 MHz, and the mission period is 1 second. We compare our proposed RAABAM and L-RAABAM with three other schemes: 1) Exhaustive search, which explores every possible user pair to find the optimal solution and serves as the upper bound for our proposed algorithms; 2) Random pairing, which randomly pairs all users; and 3) Channel-gain-based algorithm [21], which successively pairs the user with the highest channel gain with the user with the lowest channel

Algorithm 6 Low-complexity RAABAM (L-RAABAM).

1. Execute Algorithm 4 separately for the reflection and transmission spaces;
2. Set the index number for decoding order as $n = 1$;
3. **while** $n \leq 2^{I/2}$ **do**
4. Initialize $\mathbf{p}, \mathbf{f}, \mathbf{u}_{\mathrm{RIS}}^{D/U}, \tau$, and set $l = 1$;
5. **repeat**
6. Update $\tau^{(l)}$ based on (13);
7. **for** user pairs in two spaces **do**
8. Update $\mathbf{f}^{(l)}$ based on (14);
9. Update $\mathbf{p}^{(l)}$ based on (31);
10. **end for**
11. Update $\mathbf{u}^{(l)}$ based on Algorithm 2;
12. Update the iterative index $l = l + 1$;
13. **until** the objective function of (P6) converges;
14. $n = n + 1$;
15. **end while**
16. **Output** $\boldsymbol{\pi}^* = \arg\max F_{(p6)}(n)$ and the corresponding $\{\mathbf{p}, \mathbf{f}, \mathbf{u}, \tau, \boldsymbol{\delta}\}$.

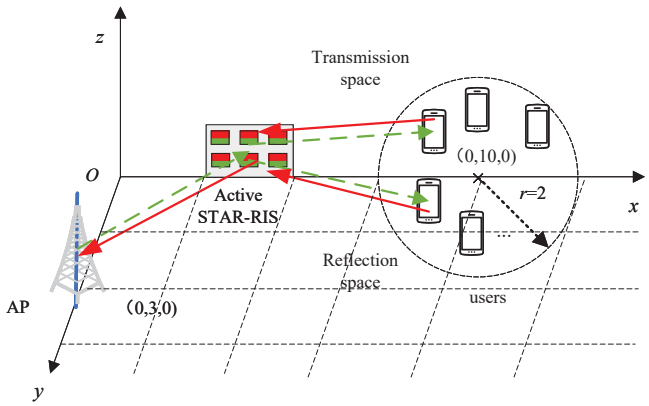

Fig. 3. The simulation setup.

gain. Other simulation parameters are listed in Table I for clarity.

Fig. 4 illustrates the convergence behavior of the proposed algorithms for both two-user and multi-user scenarios. It is assumed that there are 8 users when running the proposed RAABAM and L-RAABAM (i.e., Algorithms 5 and 6). It can be seen that for all three algorithms, the total number of completed task bits monotonically increases and stabilizes after approximately 5-6 iterations, which verifies our proposed algorithms converge fast.

Fig. 5 shows the average runtime of user pairing versus the number of users. When the number of users increases, the runtime of the channel-gain-based algorithm remains nearly constant, since the channel-gain-based algorithm only requires sorting users according to their channel gains. In contrast, the runtime of the RAABAM and L-RAABAM algorithms increase with the number of users. This is because both the number of user proposals in Initialization and the number of swap operations in Swapping Process increase with the increase of the number of users. By modifying the user

TABLE I
SIMULATION PARAMETERS [43], [44]

Parameters	Default Values
Bandwidth, B	1 MHz
Noise power, n_{AP}^2, n_{RIS}^2	-80 dBm
Rician factor, ϖ_{AP}^D, ϖ_{RIS}^D	3 dB
Maximum CPU frequency, $F_{\max}$	1 GHz
Effective capacitance coefficient, κ	10^{-28}
The tolerant threshold, ε	10^{-4}
Maximum amplitude coefficient, $\beta_{\max}$	5
Energy budget of STAR-RIS, E_{RIS}	50 dBm
Energy harvesting parameters, υ, ψ, ϕ	0.0233, 132.8, 0.0118

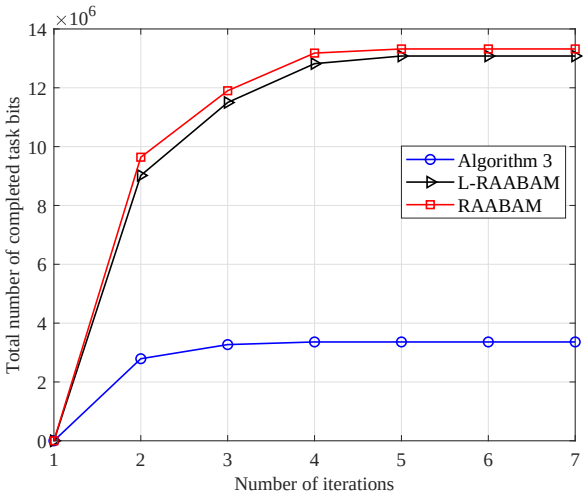

Fig. 4. The convergence behavior of proposed algorithms.

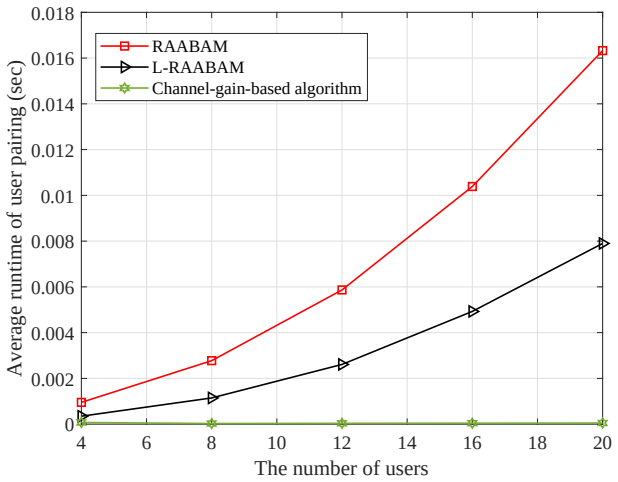

Fig. 5. The average runtime of user pairing versus the number of users

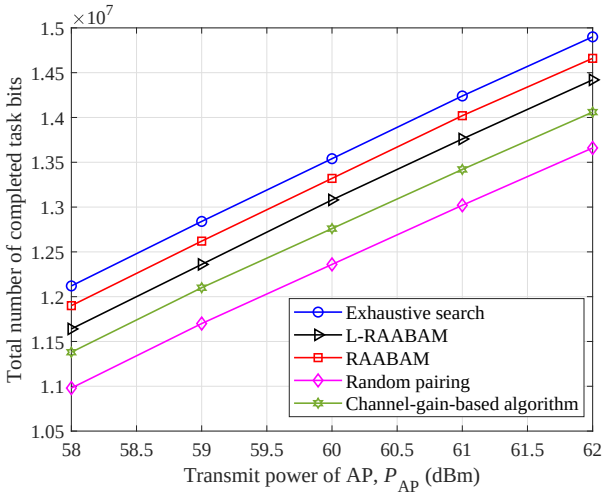

Fig. 6. The total number of completed task bits versus P_{AP}.

pairing strategy, the proposed L-RAABAM algorithm achieves a substantial reduction in runtime, thereby enabling more efficient user pairing.

Fig. 6 shows the total number of completed task bits versus the transmit power of the AP. It can be observed that as the AP's transmit power increases, the total number of completed task bits also increases. This is because with larger AP's transmit power, users can harvest more energy for local computing and task offloading. By optimizing the user pairing strategy based on matching theory, our proposed RAABAM and L-RAABAM achieve a greater total number of completed task bits than random pairing and channel-gain-based algorithms. For example, when the transmit power of the AP is 60 dBm, compared to the random pairing and channel-gain-based algorithms, the proposed RAABAM improve the total number of completed task bits by 7.76% and 4.39%, respectively. As expected, RAABAM performs better than L-RAABAM since matching users across the full space is more likely to find a better solution than matching them within reflection or transmission space separately. Thus, RAABAM can manage the inter-user interference of NOMA more effectively and achieve higher offloading data rate.

Fig. 7 shows the total number of completed task bits versus the number of STAR-RIS's elements. With the assistance of STAR-RIS, users and the AP can coherently combine the energy-carrying signals and task offloading signals reflected/transmitted by all STAR-RIS's elements respectively. Thus, when the number of STAR-RIS's elements increases, higher channel gains can be achieved for both uplink task offloading and downlink energy transfer. The improved downlink channel gains can provide users with more energy for task offloading and local computing, while the enhanced uplink channel gains improve the offloading data rate. As a result, it can be observed from Fig. 7 that the total number of completed task bits within the mission period increases with the growth of the number of elements. Additionally, we note that the proposed RAABAM and L-RAABAM perform close to the exhaustive search but with much lower complexity, which verifies the effectiveness of the proposed algorithms.

Fig. 8 demonstrates the total number of completed task bits versus the maximum transmit power of users (i.e., $P_{\max}$). When $P_{\max}$ is below 10 dBm, users can offload task bits to the AP at the maximum transmit power. Thus, the total number of completed task bits increases as $P_{\max}$ grows. However, when $P_{\max}$ further increases, the total number of completed task bits ceases to increase since the harvested energy of users

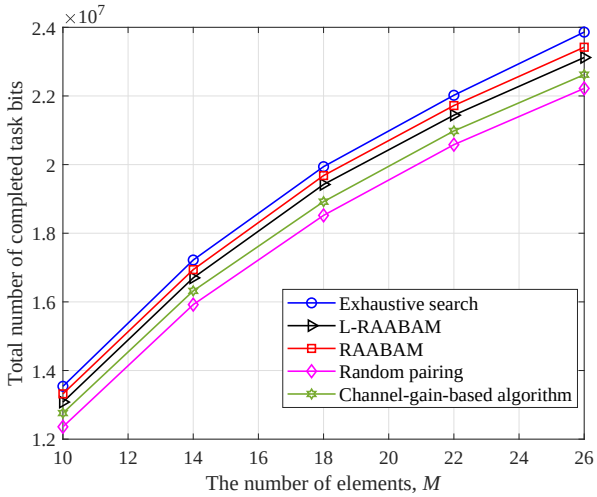

Fig. 7. The total number of completed task bits versus M.

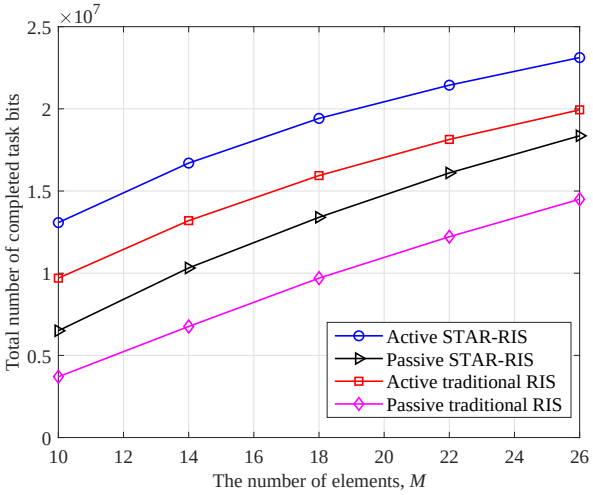

Fig. 9. The impacts of different RISs.

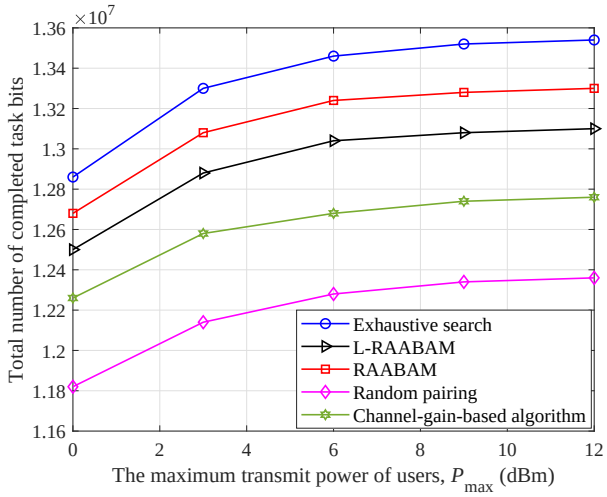

Fig. 8. The total number of completed task bits versus $P_{\max}$.

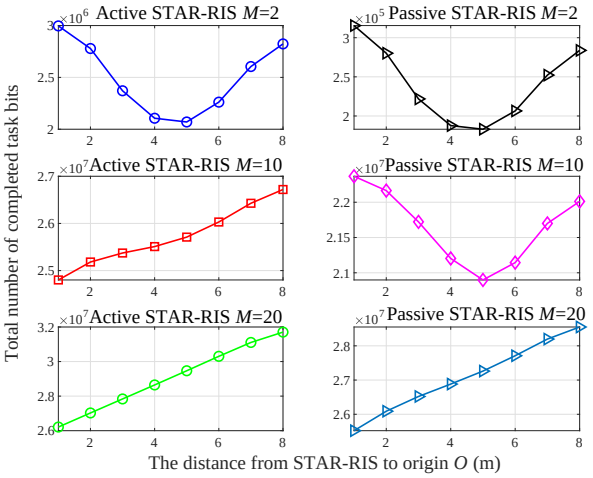

Fig. 10. The impacts of STAR-RIS's deployment location.

in the mission period is limited and users' practical transmit power for task offloading cannot reach the bound of maximum transmit power constraint.

Fig. 9 illustrates the impact of different RISs on the total number of completed task bits. Since active STAR-RIS or active traditional RIS incurs additional energy consumption when amplifying incident signals, we adjust the power of the AP in the schemes with passive STAR-RIS and passive traditional RIS as $P_{\mathrm{AP}} + E_{\mathrm{RIS}}/\tau$ for a fair comparison. On one hand, it can be found that compared to traditional RIS, the schemes with STAR-RIS can achieve better performance due to the extra DoFs provided by STAR-RIS. On the other hand, since the multiplicative fading effects can be overcome by active STAR-RIS/RIS, the active schemes perform greatly better than the passive schemes.

Fig. 10 demonstrates the impacts of the STAR-RIS's deployment location on the total number of completed task bits. From Fig. 10, we can observe that with a small number of STAR-RIS's elements ($M = 2$), the total number of completed task bits first decreases and then increases as the distance from the STAR-RIS to the origin O increases, for both passive and active STAR-RIS. This is because the offloading data rate is dominated by the cascaded channel gains between users and the AP, i.e., $\left|\mathbf{h}_{\mathrm{RIS,AP}}^{U}\mathbf{u}_{\mathrm{RIS}}^{U,e}\mathbf{h}_{i,\mathrm{RIS}}^{U}\right|^2$, which first decreases and then increases as the distance from STAR-RIS to O increases. Interestingly, when $M = 10$, passive and active STAR-RIS show different trends as the distance from the STAR-RIS to O increases. This is because the active STAR-RIS simultaneously amplifies the incident signals and noise, i.e., $n_{\mathrm{RIS}}^2\left\|\mathbf{h}_{\mathrm{RIS,AP}}^{U}\mathbf{u}_{\mathrm{RIS}}^{U,e}\right\|^2$. The amplified noise power decreases as the distance between STAR-RIS and AP increases, resulting in an increased offloading data rate as the distance from the STAR-RIS to O increases. When the number of STAR-RIS's elements further increases ($M = 20$), the unamplified noise of the passive STAR-RIS cannot be ignored. In this case, the total number of completed task bits increases as the distance from the STAR-RIS to O for both passive and active STAR-RIS increases. These results provide valuable guidance for the deployment of active/passive STAR-RIS in wireless-powered

MEC systems. For instance, to maximize the total number of completed task bits, if the number of STAR-RIS elements is small, it should be deployed near the AP or users. Conversely, it should be deployed close to users.

V. Conclusions

In this paper, we have investigated the active STAR-RIS-assisted wireless-powered MEC systems under the NOMA protocol. The active STAR-RIS was deployed to enhance the efficiency of both energy transfer and task offloading by reflecting/transmitting and amplifying signals. Beginning with a two-user scenario, we proposed RAABA to maximize the total number of completed task bits by optimizing the energy transfer time, decoding order, transmit power, CPU frequency of users, and beamforming of the active STAR-RIS. Then, by leveraging a matching-theory-based user pairing algorithm, we extended RAABA to general multi-user scenarios. Furthermore, we reduced the computational complexity of RAABAM by modifying the matching process and deriving the closed-form expression for users' transmit power, and proposed L-RAABAM. Simulation results demonstrated the effectiveness of RAABAM and L-RAABAM and provided insights for the optimal deployment locations of active STAR-RIS in wireless-powered MEC systems.

Appendix A
Proof of Theorem 1

Proof: The derivative of the objective function with respect to f_i can be derived as $\frac{T-\tau}{C_i} \geq 0$. Hence, the objective function of (P1) is a monotonic increasing function of f_i. Assume that the optimal solution to problem (P1) is $\mathbf{z}^*$. If $(T-\tau)\,{p_i}^* + \kappa\,(T-\tau)\,(f_i^*)^3 < \tau P_{\mathrm{out},i}$ and $f_i^* < F_{\max}$, we can increase f_i^* to further increase the objective function. Hence, the assumed optimal solution is not optimal. Thus, Theorem 1 is proved. ■

Appendix B
Proof of Theorem 2

Proof: The objective function of (P2) can be first transformed into

$$F(\mathbf{p},\boldsymbol{\gamma}) = \sum_{i=\{j,q\}} \omega \log(1+\gamma_i) + \frac{\omega(1+\gamma_j)p_j\left|\mathbf{h}_{\mathrm{RIS,AP}}^{U}\mathbf{u}_{\mathrm{RIS}}^{U,e}\mathbf{h}_{j,\mathrm{RIS}}^{U}\right|^2}{p_j\left|\mathbf{h}_{\mathrm{RIS,AP}}^{U}\mathbf{u}_{\mathrm{RIS}}^{U,e}\mathbf{h}_{j,\mathrm{RIS}}^{U}\right|^2+\xi_q} - \sum_{i=\{j,q\}} \omega\gamma_i + \frac{\omega(1+\gamma_q)p_q\left|\mathbf{h}_{\mathrm{RIS,AP}}^{U}\mathbf{u}_{\mathrm{RIS}}^{U,e}\mathbf{h}_{q,\mathrm{RIS}}^{U}\right|^2}{p_q\left|\mathbf{h}_{\mathrm{RIS,AP}}^{U}\mathbf{u}_{\mathrm{RIS}}^{U,e}\mathbf{h}_{q,\mathrm{RIS}}^{U}\right|^2+n_{\mathrm{RIS}}^2\left\|\mathbf{h}_{\mathrm{RIS,AP}}^{U}\mathbf{u}_{\mathrm{RIS}}^{U,e}\right\|^2+n_{\mathrm{AP}}^2}. \tag{32}$$

It can be found that $F(\mathbf{p},\boldsymbol{\gamma})$ is a concave and differentiable function over γ_i when p_i is fixed. Thus, γ_i can be optimally determined by setting the derivative of $F(\mathbf{p},\boldsymbol{\gamma})$ with respect to γ_i as zero. By doing so, we can obtain

$$\gamma_j^* = \frac{p_j\left|\mathbf{h}_{\mathrm{RIS,AP}}^{U}\mathbf{u}_{\mathrm{RIS}}^{U,e}\mathbf{h}_{j,\mathrm{RIS}}^{U}\right|^2}{p_q\left|\mathbf{h}_{\mathrm{RIS,AP}}^{U}\mathbf{u}_{\mathrm{RIS}}^{U,e}\mathbf{h}_{q,\mathrm{RIS}}^{U}\right|^2+n_{\mathrm{RIS}}^2\left\|\mathbf{h}_{\mathrm{RIS,AP}}^{U}\mathbf{u}_{\mathrm{RIS}}^{U,e}\right\|^2+n_{\mathrm{AP}}^2}, \quad \gamma_q^* = \frac{p_q\left|\mathbf{h}_{\mathrm{RIS,AP}}^{U}\mathbf{u}_{\mathrm{RIS}}^{U,e}\mathbf{h}_{q,\mathrm{RIS}}^{U}\right|^2}{n_{\mathrm{RIS}}^2\left\|\mathbf{h}_{\mathrm{RIS,AP}}^{U}\mathbf{u}_{\mathrm{RIS}}^{U,e}\right\|^2+n_{\mathrm{AP}}^2}. \tag{33}$$

Then, by substituting γ_j^* and γ_q^* into (32), we can obtain $F(\mathbf{p},\gamma^*)$ which is the same with the objective function of (P2). Therefore, the equivalence between (32) and (P2) is established. Next, with fixed $\boldsymbol{\gamma}$, we apply the quadratic transform to the two ratio terms in (32), and (32) can be rewritten as the objective function of (P3) (referred to as $G(\mathbf{p},\boldsymbol{\gamma},\mathbf{y})$). $G(\mathbf{p},\boldsymbol{\gamma},\mathbf{y})$ is also concave with respect to y_i. Similar to $\boldsymbol{\gamma}$, by setting $\nabla_{\mathbf{y}} G$ to 0, we can obtain

$$y_j^* = \frac{\omega(1+\gamma_j)p_j\left|\mathbf{h}_{\mathrm{RIS,AP}}^{U}\mathbf{u}_{\mathrm{RIS}}^{U,e}\mathbf{h}_{j,\mathrm{RIS}}^{U}\right|^2}{p_j\left|\mathbf{h}_{\mathrm{RIS,AP}}^{U}\mathbf{u}_{\mathrm{RIS}}^{U,e}\mathbf{h}_{j,\mathrm{RIS}}^{U}\right|^2+\xi_q}, \quad y_q^* = \frac{\omega(1+\gamma_q)p_q\left|\mathbf{h}_{\mathrm{RIS,AP}}^{U}\mathbf{u}_{\mathrm{RIS}}^{U,e}\mathbf{h}_{q,\mathrm{RIS}}^{U}\right|^2}{p_q\left|\mathbf{h}_{\mathrm{RIS,AP}}^{U}\mathbf{u}_{\mathrm{RIS}}^{U,e}\mathbf{h}_{q,\mathrm{RIS}}^{U}\right|^2+n_{\mathrm{RIS}}^2\left\|\mathbf{h}_{\mathrm{RIS,AP}}^{U}\mathbf{u}_{\mathrm{RIS}}^{U,e}\right\|^2+n_{\mathrm{AP}}^2}. \tag{34}$$

By substituting (34) into (P3), $G(\mathbf{p},\boldsymbol{\gamma},\mathbf{y})$ can recover as the form of (32), which means the equivalence between (32) and (P3). Therefore, (P2) is equivalent to (P3). The conclusion in Theorem 2 is proved. ■

Appendix C
Proof of Theorem 3

Proof: When $\boldsymbol{\gamma}$ and $\mathbf{y}$ are given, problem (P3) is a convex optimization problem, since the objective function is concave with respect to p_i and all constraints are linear. Therefore, we can adopt the Lagrangian dual method to derive its closed-form solution. The Lagrangian function of problem (P3) can be expressed as

$$\begin{aligned} L(\Lambda) = &\sum_{i=\{j,q\}} 2y_i\sqrt{(1+\gamma_i)\,\omega p_i\left|\mathbf{h}_{\mathrm{RIS,AP}}^{U}\mathbf{u}_{\mathrm{RIS}}^{U,e}\mathbf{h}_{i,\mathrm{RIS}}^{U}\right|^2} \\ &-y_j^2\left(p_j\left|\mathbf{h}_{\mathrm{RIS,AP}}^{U}\mathbf{u}_{\mathrm{RIS}}^{U,e}\mathbf{h}_{j,\mathrm{RIS}}^{U}\right|^2+\xi_q\right) \\ &-y_q^2(p_q\left|\mathbf{h}_{\mathrm{RIS,AP}}^{U}\mathbf{u}_{\mathrm{RIS}}^{U,e}\mathbf{h}_{q,\mathrm{RIS}}^{U}\right|^2+n_{\mathrm{RIS}}^2\left\|\mathbf{h}_{\mathrm{RIS,AP}}^{U}\mathbf{u}_{\mathrm{RIS}}^{U,e}\right\|^2+n_{\mathrm{AP}}^2) \\ &+\eta\,(\Psi-E_{\mathrm{RIS}})+\mathrm{T}, \end{aligned} \tag{35}$$

where $\Lambda=\{p_j,p_q,\eta\}$. $\mathrm{T}=\sum_{i=\{j,q\}}(\omega\log(1+\gamma_i)-\omega\gamma_i)$. Then, by setting the derivation of $L(\Lambda)$ with respect to $p_i, i\in\{j,q\}$ as 0, we can obtain

$$p_i^* = \frac{y_i^2\,(1+\gamma_i)\,\omega\left|\mathbf{h}_{\mathrm{RIS,AP}}^{U}\mathbf{u}_{\mathrm{RIS}}^{U,e}\mathbf{h}_{i,\mathrm{RIS}}^{U}\right|^2}{\left(y_i^2\left|\mathbf{h}_{\mathrm{RIS,AP}}^{U}\mathbf{u}_{\mathrm{RIS}}^{U,e}\mathbf{h}_{i,\mathrm{RIS}}^{U}\right|^2-\eta\sum_{e=\{r,t\}}\left\|\mathbf{u}_{\mathrm{RIS}}^{U,e}\mathbf{h}_{i,\mathrm{RIS}}^{U}\right\|^2\right)^2}. \tag{36}$$

Finally, taking the constraints C1, C6, and (15c) into account, the optimal transmit power of user i and user j can be given by (17). The conclusion in Theorem 3 is proved. ■

Appendix D
Proof of Theorem 4

Proof: In problem (P2), if user j and user q are located at the same side of STAR-RIS, the derivatives of the objective function with respect to p_j and p_q can be given by $D_j = \frac{\left|\mathbf{h}_{\mathrm{RIS,AP}}^{U}\mathbf{u}_{\mathrm{RIS}}^{U,e}\mathbf{h}_{j,\mathrm{RIS}}^{U}\right|^2}{p_j\left|\mathbf{h}_{\mathrm{RIS,AP}}^{U}\mathbf{u}_{\mathrm{RIS}}^{U,e}\mathbf{h}_{j,\mathrm{RIS}}^{U}\right|^2+\xi_q}$ and $D_q = \frac{\left|\mathbf{h}_{\mathrm{RIS,AP}}^{U}\mathbf{u}_{\mathrm{RIS}}^{U,e}\mathbf{h}_{q,\mathrm{RIS}}^{U}\right|^2}{p_j\left|\mathbf{h}_{\mathrm{RIS,AP}}^{U}\mathbf{u}_{\mathrm{RIS}}^{U,e}\mathbf{h}_{j,\mathrm{RIS}}^{U}\right|^2+\xi_q}$, respectively. It is obvious that both D_j and D_q are non-negative. Thus, the objective function of (P2) is monotonically increasing with respect to p_j and p_q. For constraint C2, since E_{RIS} is large enough, C2 always holds even when p_j and p_q reach their maximum values within the feasible region. Therefore, considering C1, C6, and (15c), the optimal

solutions for p_j and p_q are given by (31). This proves the conclusion in Theorem 4. ■

REFERENCES

[1] M. Sharma, A. Tomar, and A. Hazra, "Edge computing for industry 5.0: Fundamental, applications, and research challenges," *IEEE Internet Things J.*, vol. 11, no. 11, pp. 19 070–19 093, Jun. 2024.

[2] D. Patil, M. K. McDonough *et al.*, "Wireless power transfer for vehicular applications: Overview and challenges," *IEEE Trans. Transp. Electrif.*, vol. 4, no. 1, pp. 3–37, Mar. 2018.

[3] X. Li, T. Jing *et al.*, "Two-stage offloading for an enhancing distributed vehicular edge computing and networks: Model and algorithm," *IEEE Trans. Intell. Transp. Syst.*, vol. 25, no. 11, pp. 17 744–17 761, Nov. 2024.

[4] J. Akhter, R. Hazra *et al.*, "A novel resource sharing scheme for vehicular communication in 5G cellular networks for smart cities," *IEEE Trans. Consum. Electron.*, DOI: 10.1109/TCE.2024.3392435 2024.

[5] J. J. Astrain, F. Falcone *et al.*, "Monitoring of electric buses within an urban smart city environment," *IEEE Sens. J.*, vol. 22, no. 12, pp. 11 364–11 372, Jun. 2022.

[6] Q. You, C. Gao *et al.*, "A seamlessly integrated device of wireless energy storage and humidity sensing for human-machine interaction of respiration," *Small*, vol. 21, no. 13, Art. no. 2501122, Mar. 2025.

[7] C. Zhong and X. Nie, "Feasibility of LoRa for smart home: Real time and coverage considerations," *IEEE Internet of Things J.*, vol. 11, no. 14, pp. 25 213–25 226, Jul. 2024.

[8] W. Saad, M. Bennis, and M. Chen, "A vision of 6G wireless systems: Applications, trends, technologies, and open research problems," *IEEE Netw.*, vol. 34, no. 3, pp. 134–142, May 2020.

[9] S. Bi *et al.*, "Computation rate maximization for wireless powered mobile-edge computing with binary computation offloading," *IEEE Trans. Wireless Commun.*, vol. 17, no. 6, pp. 4177–4190, Jun. 2018.

[10] L. Shi, Y. Ye, X. Chu, and G. Lu, "Computation energy efficiency maximization for a NOMA-based WPT-MEC network," *IEEE Internet of Things J.*, vol. 8, no. 13, pp. 10 731–10 744, Jul. 2021.

[11] X. Jiao *et al.*, "Deep reinforcement learning empowers wireless powered mobile edge computing: Towards energy-aware online offloading," *IEEE Trans. Commun.*, vol. 71, no. 9, pp. 5214–5227, Sep. 2023.

[12] X. Chen, W. Dai *et al.*, "Augmented deep reinforcement learning for online energy minimization of wireless powered mobile edge computing," *IEEE Trans. Commun.*, vol. 71, no. 5, pp. 2698–2710, May 2023.

[13] A. Gao, S. Zhang *et al.*, "Game-combined multi-agent DRL for tasks offloading in wireless powered MEC networks," *IEEE Trans. Veh. Technol.*, vol. 72, no. 7, pp. 9131–9144, Jul. 2023.

[14] Y. Liu, X. Liu *et al.*, "Reconfigurable intelligent surfaces: Principles and opportunities," *IEEE Commun. Surv. Tutor.*, vol. 23, no. 3, pp. 1546–1577, thirdquarter 2021.

[15] Q. Zhang, Y. Wang, H. Li, S. Hou, and Z. Song, "Resource allocation for energy efficient STAR-RIS aided MEC systems," *IEEE Wirel. Commun. Lett.*, vol. 12, no. 4, pp. 610–614, Apr. 2023.

[16] M. Bian, Y. Shi, Y. Huang, and X.-W. Tang, "QoS-aware energy storage maximization in the RIS-aided joint-SWIPT-MEC system," *IEEE Commun. Lett.*, vol. 27, no. 12, pp. 3434–3438, 2023.

[17] L. Zhai, Y. Zou, and J. Zhu, "RIS-enhanced wireless powered MEC networks: A stackelberg game-based energy trading framework," in *2023 International Conference on Wireless Communications and Signal Processing (WCSP)*, 2023, pp. 488–493.

[18] Z. Yang, L. Xia *et al.*, "Delay and energy minimization for cooperative NOMA-MEC networks with SWIPT aided by RIS," *IEEE Trans. Veh. Technol.*, vol. 73, no. 4, pp. 5321–5334, Apr. 2024.

[19] X.-T. Dang, M. T. P. Le, H. V. Nguyen, S. Chatzinotas, and O.-S. Shin, "Optimal user pairing approach for NOMA-based cell-free massive MIMO systems," *IEEE Transactions on Vehicular Technology*, vol. 72, no. 4, pp. 4751–4765, Apr. 2023.

[20] R. H. Y. Perdana, T.-V. Nguyen, and B. An, "Adaptive user pairing in multi-IRS-aided massive MIMO-NOMA networks: Spectral efficiency maximization and deep learning design," *IEEE Transactions on Communications*, vol. 71, no. 7, pp. 4377–4390, Jul. 2023.

[21] S. Lv, X. Xu, S. Han, Y. Liu, P. Zhang, and A. Nallanathan, "STAR-RIS enhanced finite blocklength transmission for uplink NOMA networks," *IEEE Transactions on Communications*, vol. 72, no. 1, pp. 273–287, Jan. 2024.

[22] J. Xu, Y. Liu, X. Mu, and O. A. Dobre, "STAR-RISs: Simultaneous transmitting and reflecting reconfigurable intelligent surfaces," *IEEE Commun. Lett.*, vol. 25, no. 9, pp. 3134–3138, Sep. 2021.

[23] X. Mu, Y. Liu *et al.*, "Joint beamforming optimization for simultaneously transmitting and reflecting (STAR) RIS aided communications : (invited paper)," in *2021 55th Asilomar Conference on Signals, Systems, and Computers*, 2021, pp. 709–714.

[24] ——, "Simultaneously transmitting and reflecting (STAR) RIS aided wireless communications," *IEEE Trans. Wireless Commun.*, vol. 21, no. 5, pp. 3083–3098, May 2022.

[25] X. Mu, Z. Wang, and Y. Liu, "Simultaneously transmitting and reflecting surfaces (STARS) for multi-functional 6G," *IEEE Network*, DOI: 10.1109/MNET.2024.3481293 2024.

[26] X. Mu, J. Xu *et al.*, "Simultaneously transmitting and reflecting surfaces for ubiquitous next generation multiple access in 6G and beyond," *Proceedings of the IEEE*, DOI: 10.1109/JPROC.2024.3405351 2024.

[27] X. Qin, Z. Song *et al.*, "Joint resource allocation and configuration design for STAR-RIS-enhanced wireless-powered MEC," *IEEE Trans. Commun.*, vol. 71, no. 4, pp. 2381–2395, Apr. 2023.

[28] D.-B. Ha, V.-T. Truong *et al.*, "STAR-RIS-aided UAV NOMA Mobile Edge Computing Network with RF Energy Harvesting," *Mobile Netw Appl*, May 2024.

[29] K. Zhi, C. Pan, H. Ren, K. K. Chai, and M. Elkashlan, "Active RIS versus passive RIS: Which is superior with the same power budget?" *IEEE Commun. Lett.*, vol. 26, no. 5, pp. 1150–1154, May 2022.

[30] J. Xu, J. Zuo, J. T. Zhou, and Y. Liu, "Active Simultaneously Transmitting and Reflecting (STAR)-RISs: Modeling and Analysis," *IEEE Commun. Lett.*, vol. 27, no. 9, pp. 2466–2470, Sep. 2023.

[31] G. Li, M. Zeng *et al.*, "Latency Minimization for IRS-Aided NOMA MEC Systems With WPT-Enabled IoT Devices," *IEEE Internet of Things J.*, vol. 10, no. 14, pp. 12 156–12 168, Jul. 2023.

[32] Q. Zhang, Y. Zhao, H. Li, S. Hou, and Z. Song, "Joint optimization of STAR-RIS assisted UAV communication systems," *IEEE Wirel. Commun. Lett.*, vol. 11, no. 11, pp. 2390–2394, Nov. 2022.

[33] Z. Zhang, J. Chen *et al.*, "On the secrecy design of STAR-RIS assisted uplink NOMA networks," *IEEE Trans. Wireless Commun.*, vol. 21, no. 12, pp. 11 207–11 221, Dec. 2022.

[34] C. Zhang, W. Yi *et al.*, "STAR-IOS Aided NOMA Networks: Channel Model Approximation and Performance Analysis," *IEEE Trans. Wirel. Commun.*, vol. 21, no. 9, pp. 6861–6876, Sep. 2022.

[35] E. Boshkovska, D. W. K. Ng *et al.*, "Practical non-linear energy harvesting model and resource allocation for SWIPT systems," *IEEE Commun. Lett.*, vol. 19, no. 12, pp. 2082–2085, Dec. 2015.

[36] *Study on non-orthogonal multiple access (NOMA) for NR (Release 16)*, 3GPP Std. TR 38.812, Dec. 2018.

[37] P. Tseng, "Convergence of a block coordinate descent method for nondifferentiable minimization," *Journal of Optimization Theory and Applications*, vol. 109, pp. 475–494, 2001.

[38] Z. Yang, C. Pan *et al.*, "Energy efficient resource allocation in UAV-enabled mobile edge computing networks," *IEEE Trans. Wireless Commun.*, vol. 18, no. 9, pp. 4576–4589, Sep. 2019.

[39] J. Cui, Y. Liu *et al.*, "Optimal user scheduling and power allocation for millimeter wave NOMA systems," *IEEE Trans. Wireless Commun.*, vol. 17, no. 3, pp. 1502–1517, Mar. 2018.

[40] J. Zuo, Y. Liu, Z. Qin, and N. Al-Dhahir, "Resource allocation in intelligent reflecting surface assisted NOMA systems," *IEEE Transactions on Communications*, vol. 68, no. 11, pp. 7170–7183, Nov. 2020.

[41] J. Zhao, Y. Liu *et al.*, "Spectrum allocation and power control for non-orthogonal multiple access in hetnets," *IEEE Trans. Wireless Commun.*, vol. 16, no. 9, pp. 5825–5837, Sep. 2017.

[42] K. Wang, Y. Liu *et al.*, "User association and power allocation for multi-cell non-orthogonal multiple access networks," *IEEE Trans. Wirel. Commun.*, vol. 18, no. 11, pp. 5284–5298, Nov. 2019.

[43] S. Mao *et al.*, "Computation rate maximization for intelligent reflecting surface enhanced wireless powered mobile edge computing networks," *IEEE Trans. Veh. Technol.*, vol. 70, no. 10, pp. 10 820–10 831, Oct. 2021.

[44] C. Luo *et al.*, "Reconfigurable intelligent sensing surface aided wireless powered communication networks: A sensing-then-reflecting approach," *IEEE Trans. Commun.*, vol. 72, no. 3, pp. 1835–1848, Mar. 2024.

Xintong Qin received the B.Sc. degree from the School of Electronic and Information Engineering, Beijing Jiaotong University, Beijing, China, in 2020, where he is currently pursuing the Ph.D. degree. His research interests are in the field of nonorthogonal multiple access, mobile edge computing, unmanned aerial vehicle, and reconfigurable intelligent surfaces.

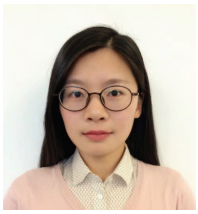

Wenjuan Yu (Member, IEEE) received her Ph.D. degree in Communication Systems from Lancaster University, Lancaster, U.K. She is currently a Lecturer with the School of Computing and Communications (SCC), InfoLab21, Lancaster University. She was a Research Fellow with the 5G Innovation Centre (5GIC), Institute for Communication Systems, University of Surrey, UK, from 2018 to 2020. Prior to that, she worked as a part-time Research Officer at the School of Computer Science and Electronic Engineering, University of Essex, UK, from Aug 2017 to Jan 2018. Her research interests include radio resource management, low latency communications, and machine learning for communications. She was an Executive Editor of the Transactions on Emerging Telecommunications Technologies from 2019 to 2022. She served as the lead Co-Chair for NGMA workshop in IEEE VTC2023-Spring and also a TPC Member for many conferences such as IEEE GLOBECOM, IEEE ICC, and IEEE VTC. She is the Conference Symposium and Workshop Officer for the Next Generation Multiple Access Emerging Technology Initiative (NGMA-ETI).

Qiang Ni (Senior Member, IEEE) is currently a Professor and the Head of the Communication Systems Group, School of Computing and Communications, Lancaster University, Lancaster, U.K. His research interests include the area of future generation communications and networking, including green communications and networking, millimeter-wave wireless communications, cognitive radio network systems, non-orthogonal multiple access (NOMA), heterogeneous networks, 5G and 6G, SDN, cloud networks, energy harvesting, wireless information and power transfer, IoTs, cyber physical systems, AI and machine learning, big data analytics, and vehicular networks. He has authored or co-authored 300+ papers in these areas. He was an IEEE 802.11 Wireless Standard Working Group Voting Member and a contributor to various IEEE wireless standards.

Zhengyu Song (Member, IEEE) received the B.Sc. and M.Sc. degrees in information and communication engineering from Beijing Jiaotong University, Beijing, China, in 2008 and 2011, respectively, and the Ph.D. degree in information and communication engineering from the Beijing Institute of Technology, Beijing, in 2016. He is currently with the School of Electronic and Information Engineering, Beijing Jiaotong University. His main research interests include nonorthogonal multiple access, mobile-edge computing, reconfigurable intelligent surfaces, unmanned aerial vehicle, and terrestrial-satellite-integrated communications.

Tianwei Hou (Member, IEEE) received the Ph.D. degree from Beijing Jiaotong University (BJTU) in 2021. He was a visiting scholar at Queen Mary University of London (QMUL) (Sep. 2018- Nov. 2020). Since 2021, he has been an associate professor at BJTU. Dr. Hou's current research interests include next generation multiple access (NGMA), reconfigurable intelligent surface (RIS) aided communications, UAV communications, multiuser multiple-input multiple-output (MIMO) communications, and stochastic geometry. He received the Exemplary Reviewer of the IEEE COMMUNICATION LETTERS and the IEEE TRANSACTIONS ON COMMUNICATIONS in 2018 and 2019. He has served as a TPC Member for many IEEE conferences, such as GLOBECOM, VTC, etc. He served as the publicity officer for the Next Generation Multiple Access Emerging Technology Initiative. He has served as the Co-Chair in workshop for VTC 2022-Fall, VTC 2023-Spring and ISCT-2022.

Jun Wang received the B.Sc. degree in electronic information engineering and the Ph.D. degree in signal processing from Beijing Institute of Technology in 2004 and 2011, respectively. Then, he was a postdoctoral researcher in Beijing Jiaotong University. He is currently an associate professor with Beijing Jiaotong University, Beijing, China. His research interests include signal processing in wireless communication and satellite navigation systems.

Xin Sun received the Ph.D. degree in electromagnetic measurement technology and instrument from Harbin Institute of Technology, Harbin, China, in 1998. She is currently a Professor with the School of Electronic and Information Engineering, Beijing Jiaotong University, Beijing, China. Her main research interests are professional mobile communications, wireless personal communications, green networking, and satellite communications.